

Accurate Time Integration of Linear Elastodynamics Problems

A. Idesman¹

Abstract: The paper deals with the following issues of existing time-integration methods for a semi-discrete system of elastodynamics equations: a) the quantification and the suppression of spurious high frequencies; b) the selection of the amount of numerical dissipation for a time-integration method; and c) accurate time integration of low modes. The finite element method used in the paper or other methods can be applied for the space discretization. A new two-stage time-integration procedure consisting of basic computations and the filtering stage is developed. For accurate integration of all frequencies, a time-integration method with zero (or small) numerical dissipation is applied for basic computations which allow spurious high-frequency oscillations. To filter these oscillations, pre- or/and post-processing is applied using a time-integration method with large numerical dissipation. New implicit first-order and explicit second-order time-continuous Galerkin (TCG) methods with large numerical dissipation are developed for the filtering stage of the two-stage time-integration procedure. A new general expression related to the selection of the minimum necessary amount of numerical dissipation (in terms of a time increment) for pre- or post-processing is suggested. The application of the two-stage time-integration procedure to 1-D and 2-D elastodynamics problems shows its effectiveness. Using the two-stage time-integration procedure, wave propagation and structural dynamics problems are uniformly solved. In contrast to existing approaches that use a method with the same dissipation (or artificial viscosity) for all calculations, the new technique requires no interaction between user and computer code for wave propagation and impact problems (the selection of the size of time increments for existing time-integration methods with numerical dissipation is an issue and is user-defined) and yields accurate and non-oscillatory results.

Keywords: elastodynamics, elastic waves, spurious oscillations, time integration, numerical dissipation, finite elements

¹ Texas Tech University, Lubbock, TX, USA.

1 Introduction

The application of finite elements in space to linear elastodynamics problems leads to a system of ordinary differential equations in time

$$\mathbf{M}\ddot{\mathbf{U}} + \mathbf{C}\dot{\mathbf{U}} + \mathbf{K}\mathbf{U} = \mathbf{R}, \quad (1)$$

where \mathbf{M} , \mathbf{C} , \mathbf{K} are the mass, damping, and stiffness matrices, respectively, \mathbf{U} is the vector of the nodal displacement, \mathbf{R} is the vector of the nodal load. Eq. (1) can also be obtained by the application of different discretization methods in space such as the spectral element method, the boundary element method, the smoothed particle hydrodynamics method and others. Many different numerical methods have been developed for the time integration of Eq. (1). However, for wave propagation problems even the exact integration of Eq. (1) leads to the appearance of spurious high-frequency oscillations. We should emphasize that the goal of calculations is not an accurate integration of Eq. (1) but accurate solutions of original elastodynamics problems before the space discretization. There are no reliable time-integration methods for the integration of Eq. (1) that yield accurate solutions of original elastodynamics problems (described by partial differential equations) without spurious oscillations. Existing time-integration methods (e.g., the Houbolt method, the Newmark method, the Wilson- Θ method, the Park method, and the HHT- α method, time-discontinuous and time-continuous Galerkin methods and many others, see Zienkiewicz and Taylor (2000); Hughes (1987); Bathe (1996)) treat this issue by the introduction of numerical dissipation (or artificial viscosity) for all time increments at integration of Eq. (1) in order to suppress spurious high-frequency oscillations. However, we have not seen in the literature any recommendations related to the selection of the amount of numerical dissipation, which should be expressed in terms of the size of a time increment and some other parameters. Moreover, it is not clear whether these methods can filter all spurious oscillations even for some benchmark elastodynamics problems. Another issue with the existing time-integration methods for linear elastodynamics is related to the fact that numerical dissipation or artificial viscosity also affects low modes of a numerical solution. This issue can be explained as follows. In the case of free vibration, the amplification matrix of a time integration method equals \mathbf{A}^n for n time increments (where \mathbf{A} is the amplification matrix for one time increment). Therefore, the spectral radius of the amplification matrix equals r^n for n time increments (where r is the spectral radius for one time increment). For accurate integration of low modes in the case of zero physical damping, the spectral radius r of the amplification matrix for low modes should be close to unity at any number of time increments. However, due to numerical dissipation or artificial viscosity, it significantly deviates from unity at a moderate number of time increments (despite the fact that the spectral radius is

close to unity for one time increment). E.g., if $r = 0.99$ for $n = 1$, then it becomes equal to $r = 0.99^{100} = 0.366$ for $n = 100$, or if $r = 0.999$ for $n = 1$, then it becomes equal to $r = 0.999^{1000} = 0.3677$ for $n = 1000$ and so on. This means that due to accumulation of numerical dissipation, low modes are integrated very inaccurately at long-term integration, and it is impossible to obtain accurate solutions for wave propagation problems even with a moderate number of time increments $n \geq 1000$ (for real-world problems, especially those solved by explicit methods, $n \geq 10^6$ and more). If numerical dissipation is not used in calculations, then spurious high-frequency oscillations spoil a numerical solution.

Several other techniques have also been proposed in order to improve the accuracy of numerical solutions for wave propagation in solids. In Holmes and Belytschko (1976) post-processing by digital filters was proposed in order to remove spurious oscillations. The digital filters in Holmes and Belytschko (1976) were applied for improvement of the solution in time for some specific points in space. A dispersion-corrected explicit integration technique based on a modified mass matrix was suggested in Krenk (2001) and others. A special selection of time increments which depends on spatial discretization and the frequency spectra of transient waves was proposed in Wang, Murti, and Valliappan (1992); Valliappan and Wang (1991). However, none of these numerical approaches damps out all spurious oscillations as well as includes the adequate quantification of the range of spurious frequencies (as shown below this range depends not only on a mesh but also on the observation time). Interesting numerical schemes such as WENO, RKDG and space-time discontinuous Galerkin methods have been proposed for a class of hyperbolic systems; see Xing and Shu (2006); Palaniappan, Haber, and Jerrard (2004); Abedi, Petracovici, and Haber (2006) and others. However, these schemes do not include Eq. (1), and thus are not appropriate for the class of problems under consideration.

To summarize, there are the following issues with existing time-integration methods for elastodynamics.

- Existing time-integration methods with numerical dissipation (or artificial viscosity) do not allow the suppression of spurious high frequencies while retaining good accuracy of low frequencies, especially at a large number of time increments.
- Due to the absence of the quantification of spurious high frequencies, there is no understanding of how to select the size of time increments and the amount of numerical dissipation in practical computations of elastodynamics problems.
- Due to mutually contradictory requirements (e.g., high accuracy and the introduction of numerical dissipation that should be large enough to suppress spurious oscillations), it is not clear how to select an optimal time-integration method among various existing methods.

- *Due to the absence of the quantification of spurious high frequencies, there is no justified cut-off frequency that from the computational point of view separates wave propagation and structural dynamics problems (e.g., the same 1-D problem in Section 5.2 can be treated as a structural dynamics or wave propagation problem depending upon a finite element mesh). Therefore, it is not clear under what specific conditions numerical dissipation should be included in a time-integration method.*

To resolve some of the issues discussed above, a new approach for the time-integration of a semi-discrete system of equations for elastodynamics, Eq. (1), is suggested. New findings of the paper include:

- a new two-stage time-integration procedure (consisting in basic computations and the filtering stage) for accurate time integration that is mathematically justified for linear elastodynamics problems (Section 2);
- new implicit and explicit TCG methods with large numerical dissipation for the filtering stage that filter all spurious oscillations and demonstrate the robustness of the two-stage time-integration procedure (Section 3);
- a new general expression related to the selection of the minimum necessary amount of numerical dissipation (in terms of a time increment) for a time-integration method used at the filtering stage of the time-integration procedure (see Eqs. (27) - (29)); this expression indirectly quantifies the range of spurious high frequencies (Section 4.1). New recommendations for the selection of the size of a time increment at basic computations (Section 4.2);
- the solutions of 1-D and 2-D elastodynamics problems showing the accuracy and effectiveness of the proposed numerical approach; in contrast to existing techniques, the new approach requires no guesswork for the selection of numerical dissipation or artificial viscosity, filters spurious high-frequency oscillations and retains the accuracy of a numerical solution (Section 5);
- new recommendations for effective numerical solutions of wave propagation and structural dynamics problems based on the two-stage time-integration procedure; the new approach can be equally applied to wave propagation and structural dynamics problems (for structural dynamics, the filtering stage may be omitted if high modes in semidiscrete equations are not excited); Section 2.3.

2 A new two-stage time-integration procedure for elastodynamics

2.1 Modal decomposition

In order to simplify the explanation and understanding of a two-stage time-integration procedure for elastodynamics, we first apply the method of modal decomposition to Eq. (1) (although the modal decomposition method is not used in calculations). In

this case, the integration of a coupled system of semi-discrete elastodynamics equations, Eq. (1) (proportional damping is assumed), reduces to the time integration of n uncoupled ordinary differential equations (e.g., see Hughes (1987))

$$\dot{v}_i(t) + 2\xi_i v_i(t) + \omega_i^2 u_i(t) = f_i(t), \quad \dot{u}_i(t) - v_i(t) = 0, \quad (2)$$

$$u_i(0) = h_i(\mathbf{U}(0)), \quad v_i(0) = g_i(\mathbf{V}(0)), \quad i = 1, 2, \dots, n \quad (3)$$

where ω_i and f_i are the natural frequency and forcing excitation, respectively, $u_i(t)$ is the displacement, $v_i(t)$ is the velocity, ξ_i is the damping ratio, n is the number of modes (the number of degrees of freedom), $u_i(0)$ and $v_i(0)$ are the initial conditions for the i -th displacement and velocity, which can be expressed in terms of the initial displacements $h_i(\mathbf{U}(0))$ and velocities $g_i(\mathbf{V}(0))$ of the original variables $\mathbf{U}(0)$ and $\mathbf{V}(0)$. The important idea of the transition from a coupled system of ordinary differential equations (1) to n uncoupled ordinary differential equations (2) consists in the fact that the time integration of Eqs. (1) and (2) with the same time-integration method will yield the same solutions; i.e., instead of the time integration of system (1), the time integration of n uncoupled ordinary differential equations (2) can be considered; see Hughes (1987); Idesman (2007b). Next, the solution of any i -th equation (2) at time t depends on the initial condition for $u_i(0)$ and $v_i(0)$ and is independent of other displacements u_j and velocities v_j for $j \neq i$. This means that all modes u_i and v_i for $i = 1, 2, \dots, n$ are integrated independently of one another. *There is no interaction between different modes i ($i = 1, 2, \dots, n$) during time integration and, therefore, spurious high-frequency modes do not affect other modes at time integration of the semi-discrete equations, Eq. (1).*

2.2 The idea of a two-stage time-integration procedure

We will resolve the issues with existing techniques with the help of a two-stage time-integration procedure which separates the accurate time integration and the filtering of spurious oscillations into two different stages. The idea of the two-stage time-integration procedure is very simple. Because there is no interaction between different modes during time integration (they are integrated independently of one another), we propose to use the most accurate time-integration method for the accurate integration of Eq. (1). Numerical dissipation (or artificial viscosity) is not required for these calculations. We refer to this stage as basic computations. This means that all modes (including high modes) are integrated very accurately and the solution may include spurious high-frequency oscillations. The accurate integration for basic computations is especially important for a long-term integration. Then, for the damping out of spurious high modes, a method with numerical dissipation (or with artificial viscosity) can be used for a number of time increments

as a pre- or/and post-processor (the filtering stage). This method can be considered as a filter of high modes. Usually, a small number of time increments is sufficient for the filtering stage, with negligible error accumulation at low modes. The suggested approach is mathematically rigorous for linear transient dynamics problems because all modes are integrated independently of one another, and the filtering of spurious modes is not needed at each time increment as in existing approaches.

2.3 New recommendations for the selection of time-integration methods

The two-stage time-integration procedure leads to the following very important conclusions and recommendations.

a) A simple criterion can be formulated for the selection of the most effective time-integration method for basic computations. Namely, among all methods with the same computational costs, a time-integration method that yields the most accurate result of integration of Eq. (1) is the most effective method for basic computations. The following general result can be drawn from the new criterion. For example, it is known that the trapezoidal rule is the most accurate time-integration method among all implicit second-order methods and that it does not require more computational costs per time increment than other implicit second-order methods. Then, according to the new criterion, the trapezoidal rule is the most effective method for basic computations of elastodynamics problems among all implicit second-order methods. It is much more difficult to make a general statement about the most effective methods for basic computations among all explicit and implicit second- and high-order methods. In this case, it is difficult to find general relationships between the accuracy of a method and computational costs per time increment, which depend on the numerical implementation of a method (e.g., use of predictor-multicorrector schemes for high-order methods), on the required accuracy of the results, and on other factors. However, in order to get accurate results for long-term integration, high-order time-integration methods are preferable to second-order methods.

b) The main requirement at the filtering stage is the effective suppression of spurious oscillations for a few time increments. Because due to a small number of time increments, error accumulation is negligible at this stage, even a method of the first order of accuracy may be competitive.

c) Some general conclusions can also be drawn for the selection of the size of time increments for elastodynamics problems. One of the ideas of the two-stage time-integration procedure is the accurate solution of a semi-discrete problem, Eq. (1), (rather than a continuous problem) for basic computations. Therefore, due to error accumulation during the time integration, the size of a time increment should depend on the total number of time increments (the larger the number of time increments, the smaller they should be in size). The typical statement in finite element

textbooks, that for explicit methods a time increment should be close to the stability limit, is not true, because the size of a time increment should depend on the total number of time increments. We will show (see Fig. 7 below) that by the use of the two-stage time-integration procedure and explicit time-integration methods with a time increment which is much smaller than the stability limit, much more accurate solutions of the original elastodynamics system of partial differential equations can be obtained even with the classical explicit central difference method.

Remark. For many elastodynamics problems, the physical damping (matrix \mathbf{C} Eq. (1)) is introduced directly in the semi-discrete formulation (e.g., proportional loading) and is not derived from the elastodynamics system of partial differential equations. Therefore, spurious high frequencies cannot be quantified with the use of the difference between the accurate solutions of the semi-discrete problem (Eq. (1)) and the original system of partial differential equations. In this case we can only postulate that we are interested in the accurate solution of Eq. (1) (i.e., the filtering stage is not necessary), or that the ranges of spurious frequencies for the problems with and without physical damping are the same (i.e., the filtering stage for the problem with non-zero damping should be used with the amount of numerical dissipation calculated for the case of zero damping).

2.4 The practical implementation of the two-stage time-integration procedure

Depending on the initial and boundary conditions, the stage of basic computations and the filtering stage can be used with the following scenarios.

- 1) If spurious high frequencies in the finite element solution are excited due to initial conditions only or due to the difference between boundary and initial conditions at the boundary, then pre-processing can be recommended for the suppression of spurious high frequencies. After pre-processing, amplitudes of high frequencies are small and do not increase during the subsequent stage of basic computations. In this case, the two-stage time-integration procedure can include pre-processing plus basic computations. In case of some spurious oscillations in the final solution, post-processing as described below can be applied as well.
- 2) If boundary conditions include and excite spurious high frequencies during the selected observation time, then basic computations with the subsequent post-processing can be used. The solutions at different observation times can be obtained by post-processing the results of basic computations at the selected observation times; i.e., calculations can include basic computations and several post-processing stages corresponding to the selected observation times.
- 3) If after some specific time the boundary conditions do not excite spurious high frequencies, then the following procedure can be recommended. Prior to this spe-

cific time, basic computations and the subsequent post-processing can be applied. Then, basic computations are again applied for the time integration up to the final observation time.

It is necessary to note that pre-processing is more convenient in calculations than other scenarios because it is applied just once at the beginning of calculations. If post-processing is used, then it should be applied each time for a specific observation time when a numerical solution is necessary.

Remark. In order to filter spurious high frequencies and to have the numerical results in the beginning and in the end of the filtering stage at the same observation times, a time-integration method at the filtering stage can be used with an even number of uniform time increments (half of them positive, the other half negative); i.e., the filtering stage does not include actual time integration (e.g., see Section 3.4.1). In this case, zero physical damping $\mathbf{C} = \mathbf{0}$, zero boundary conditions, and the initial displacements and velocities with spurious high frequencies are used. However, another scenario of the filtering stage is also possible. If the boundary conditions do not excite high frequencies, then a time-integration method at the filtering stage can be used with positive time increments. In this case, original boundary conditions are used at the filtering stage with actual integration in time.

3 Time-continuous Galerkin methods for filtering spurious high-frequency oscillations at the filtering stage

Many different time-integration methods with numerical dissipation for elastodynamics are available. Unfortunately, accuracy analysis cannot predict whether these methods will filter all spurious oscillations and will yield non-oscillatory results. For example, the numerical results available in the literature show that time-integration methods with numerical dissipation such as the *HHT* – α method, the *WBZ* – α method, different modifications of the time-discontinuous Galerkin (TDG) method and other methods (e.g., see Li and Wiberg (1998); Chien and Wu (2000); Bonelli and Bursi (2001); Mancuso and Ubertini (2003); Kunthong and Thompson (2005); Hulbert (1992); Govoni, Mancuso, and Ubertini (2006); Krenk (2006); Grosu and Harari (2007) and others) improve the numerical solutions for the 1-D impact problem, but do not remove all spurious oscillations. Below we will derive new implicit first-order and explicit second-order TCG methods for the filtering stage of the two-stage time-integration procedure that effectively filter all spurious high-frequency oscillations not only for the 1-D impact problem, but also for the more complicated multi-dimensional impact and wave propagation problems (see section 5). The derivation of the TCG methods for the filtering stage is based on a weak formulation.

3.1 Weak formulation of elastodynamics based on continuous Galerkin time-stepping method

The semidiscrete equations (1) can be rewritten as follows:

$$\mathbf{M}\dot{\mathbf{V}} + \mathbf{C}\mathbf{V} + \mathbf{K}\mathbf{U} = \mathbf{R}, \quad \mathbf{V} = \dot{\mathbf{U}}, \quad (4)$$

where $\mathbf{V}(t)$ is the vector of the nodal velocity. Eqs. (4) are a coupled system of ordinary differential equations. For the continuous Galerkin time-stepping method, we introduce a partition of the whole time interval $[0, T]$ in a not necessarily uniform fashion by $0 = t_0 < t_1 < \dots < t_n < \dots < t_N$ and define the time intervals $J_n = (t_{n-1}, t_n]$, $n = 1, \dots, N$, where $t_N = T$. A weak formulation of elastodynamics for any time interval J_n can be derived from Eqs. (4) as follows:

$$\int_{J_n} (\bar{\mathbf{v}}^T + a\dot{\bar{\mathbf{v}}}^T) [\mathbf{M}\dot{\mathbf{V}} + \mathbf{C}\mathbf{V} + \mathbf{K}\mathbf{U} - \mathbf{R}] \lambda_1(t) dt = 0, \quad (5)$$

$$\int_{J_n} (\bar{\mathbf{u}}^T + a\dot{\bar{\mathbf{u}}}^T) (\dot{\mathbf{U}} - \mathbf{V}) \lambda_2(t) dt = 0, \quad (6)$$

where $\bar{\mathbf{u}}(t)$ and $\bar{\mathbf{v}}(t)$ are the arbitrary test vector functions depending on time t (they are zero at $t = 0$); a is the scalar coefficient and has the dimension of time (e.g., s); $\lambda_1(t)$ and $\lambda_2(t)$ are the weighting scalar functions depending on time t only. At time t_{n-1} nodal displacements and velocities $\mathbf{U}(t_{n-1})$ and $\mathbf{V}(t_{n-1})$ are known from the solution for the previous time interval J_{n-1} , or from the initial conditions, and $\bar{\mathbf{u}}(t_{n-1}) = \bar{\mathbf{v}}(t_{n-1}) = \mathbf{0}$. For any time interval J_n , a local time $t^* = t - t_{n-1}$ is introduced. Time t^* varies from 0 to Δt ($\Delta t = t_n - t_{n-1}$). For convenience, for all derivations for time intervals J_n , the local time t^* will be used and will be designated as t . The advantages of using additional scalar functions $\lambda_1(t)$ and $\lambda_2(t)$ were considered in our paper Idesman (2007b).

3.2 A new implicit first-order accurate TCG method for filtering spurious high-frequency oscillations

For filtering spurious high frequencies, a method with large numerical dissipation is needed. Below we derive an implicit TCG method with large numerical dissipation from Eqs. (5) and (6) using the linear approximations in time for any time interval J_n for $\mathbf{U}(t)$, $\mathbf{V}(t)$, $\bar{\mathbf{u}}(t)$ and $\bar{\mathbf{v}}(t)$

$$\mathbf{U}(t) = \mathbf{U}_0 + \mathbf{U}_1 t, \quad \mathbf{V}(t) = \mathbf{V}_0 + \mathbf{V}_1 t, \quad \bar{\mathbf{u}}(t) = \bar{\mathbf{u}}_0 + \bar{\mathbf{u}}_1 t, \quad \bar{\mathbf{v}}(t) = \bar{\mathbf{v}}_0 + \bar{\mathbf{v}}_1 t, \quad (7)$$

where \mathbf{U}_0 and \mathbf{V}_0 are the known initial displacement and velocity, \mathbf{U}_1 and \mathbf{V}_1 are unknown vectors to be determined, $\bar{\mathbf{u}}_0 = \bar{\mathbf{v}}_0 = \mathbf{0}$, and $\bar{\mathbf{u}}_1$ and $\bar{\mathbf{v}}_1$ are arbitrary test

vectors. As shown in Idesman (2007a,b) for the implicit TCG method with the linear approximations of displacements and velocities, large numerical dissipation can be reached with the parameter a close to zero. We will use $a = 0$, which corresponds to the first order of accuracy of the TCG method. To add more numerical dissipation, the following functions $\lambda_1(t) = \lambda_2(t) = t^m$ will be used in Eqs. (5) and (6) (these functions do not change the order of accuracy but affect numerical dissipation). When Eqs. (7) are inserted into Eqs. (5) and (6), the final discrete system of algebraic equations for unknowns \mathbf{U}_1 and \mathbf{V}_1 is derived as follows:

$$(\mathbf{M} + a_1\mathbf{C} + a_1^2\mathbf{K})\mathbf{U}_1 = -a_1\mathbf{K}\mathbf{U}_0 + \mathbf{M}\mathbf{V}_0 + \mathbf{R}_1, \tag{8}$$

$$\mathbf{V}_1 = \frac{1}{a_1}\mathbf{U}_1 - \frac{1}{a_1}\mathbf{V}_0, \tag{9}$$

where

$$a_1 = \frac{m+2}{m+3}\Delta t, \quad \mathbf{R}_1 = \frac{(m+2)^2}{(m+3)\Delta t^{m+1}} \int_0^{\Delta t} \mathbf{R}(t)t^{m+1} dt. \tag{10}$$

Here m is the parameter responsible for the amount of numerical dissipation (see the accuracy analysis below). After finding \mathbf{U}_1 from Eq. (8), vectors \mathbf{U} and \mathbf{V} at the end of the increment $t = \Delta t$ can be calculated as (see Eqs. (7) and (9))

$$\mathbf{U}(\Delta t) = \mathbf{U}_0 + \mathbf{U}_1\Delta t, \quad \mathbf{V}(\Delta t) = (1 - \frac{\Delta t}{a_1})\mathbf{V}_0 + \frac{\Delta t}{a_1}\mathbf{U}_1. \tag{11}$$

The derived method reduces to the following step-by-step solution scheme. For the given Δt and m , it is necessary to calculate a_1 and \mathbf{R}_1 using Eqs. (10), then for the given $\mathbf{U}_0, \mathbf{V}_0$ to solve a system of equations (8), and finally to find \mathbf{U} and \mathbf{V} at the end of the increment $t = \Delta t$ using Eqs. (11). The computational cost of the implicit TCG method is the same as that for the implicit Newmark’s method.

3.3 A new explicit second-order accurate method for filtering spurious high-frequency oscillations

For the derivation of an explicit second-order TCG method with large numerical dissipation, the quadratic time approximations of $\mathbf{U}(t), \mathbf{V}(t), \bar{\mathbf{u}}(t)$ and $\bar{\mathbf{v}}(t)$ are used

$$\begin{aligned} \mathbf{U}(t) &= \mathbf{U}_0 + \mathbf{U}_1t + \mathbf{U}_2t^2, & \mathbf{V}(t) &= \mathbf{V}_0 + \mathbf{V}_1t + \mathbf{V}_2t^2, \\ \bar{\mathbf{u}}(t) &= \bar{\mathbf{u}}_0 + \bar{\mathbf{u}}_1t + \bar{\mathbf{u}}_2t^2, & \bar{\mathbf{v}}(t) &= \bar{\mathbf{v}}_0 + \bar{\mathbf{v}}_1t + \bar{\mathbf{v}}_2t^2, \end{aligned} \tag{12}$$

where \mathbf{U}_0 and \mathbf{V}_0 are the known initial displacement and velocity, $\mathbf{U}_1, \mathbf{U}_2, \mathbf{V}_1, \mathbf{V}_2$ are unknown vectors to be determined, $\bar{\mathbf{u}}_0 = \bar{\mathbf{v}}_0 = \mathbf{0}$, and $\bar{\mathbf{u}}_1, \bar{\mathbf{u}}_2, \bar{\mathbf{v}}_1, \bar{\mathbf{v}}_2$ are arbitrary

test vectors. We will also take $a = \infty$ and $\lambda_1(t) = \lambda_2(t) = 1 + ct$ in Eqs. (5) and (6) where parameter c (as seen from the accuracy analysis; see below) is responsible for numerical dissipation. Then Eqs. (5) and (6) can be rewritten as follows:

$$\int_{J_n} \dot{\mathbf{v}}^T [\mathbf{M}\dot{\mathbf{V}} + \mathbf{C}\mathbf{V} + \mathbf{K}\mathbf{U} - \mathbf{R}] (1 + ct) dt = 0, \quad (13)$$

$$\int_{J_n} \dot{\mathbf{u}}^T (\dot{\mathbf{U}} - \mathbf{V}) (1 + ct) dt = 0. \quad (14)$$

For the transition from Eqs. (5) and (6) to Eqs. (13) and (14), we divided the former equations by a and considered the limit $a = \infty$. For simplicity, the case of zero physical damping ($\mathbf{C} = \mathbf{0}$) is considered. Substituting Eqs. (12) into Eq. (14), we can find that

$$\mathbf{V}_1 = 2\mathbf{U}_2 + a_1\mathbf{U}_1 - a_1\mathbf{V}_0, \quad \mathbf{V}_2 = a_2\mathbf{U}_1 - a_2\mathbf{V}_0, \quad (15)$$

with

$$a_1 = \frac{60 + 64c\Delta t + 12c^2\Delta t^2}{\Delta t(10 + 12c\Delta t + 3c^2\Delta t^2)}, \quad a_2 = -\frac{10(6 + 6c\Delta t + c^2\Delta t^2)}{\Delta t^2(10 + 12c\Delta t + 3c^2\Delta t^2)}. \quad (16)$$

Substituting Eqs. (12) into Eq. (13) and using Eqs. (15) and (16), we have

$$\begin{aligned} & \mathbf{M}\mathbf{U}_1 - \frac{\Delta t^2(10 + 12c\Delta t + 3c^2\Delta t^2)}{20(6 + 6c\Delta t + c^2\Delta t^2)}\mathbf{K}\mathbf{U}_1 \\ & - \frac{\Delta t^3(10 + 12c\Delta t + 3c^2\Delta t^2)(15 + 16c\Delta t + 3c^2\Delta t^2)}{50(6 + 6c\Delta t + c^2\Delta t^2)^2} \frac{\Delta t^3}{12}\mathbf{K}\mathbf{U}_2 = \mathbf{M}\mathbf{V}_0 \\ & + \frac{3\Delta t(3 + 2c\Delta t)(10 + 12c\Delta t + 3c^2\Delta t^2)}{5(6 + 6c\Delta t + c^2\Delta t^2)^2}\mathbf{R}_1 - \frac{9\Delta t(2 + c\Delta t)(10 + 12c\Delta t + 3c^2\Delta t^2)}{10(6 + 6c\Delta t + c^2\Delta t^2)^2}\mathbf{R}_2, \end{aligned} \quad (17)$$

$$\begin{aligned} & \mathbf{M}\mathbf{U}_2 + \frac{\Delta t(90 + 186c\Delta t + 129c^2\Delta t^2 + 34c^3\Delta t^3 + 3c^4\Delta t^4)}{10(6 + 6c\Delta t + c^2\Delta t^2)^2}\mathbf{K}\mathbf{U}_1 \\ & + \frac{\Delta t^2(600 + 1260c\Delta t + 884c^2\Delta t^2 + 234c^3\Delta t^3 + 21c^4\Delta t^4)}{100(6 + 6c\Delta t + c^2\Delta t^2)^2}\mathbf{K}\mathbf{U}_2 = -\frac{1}{2}\mathbf{K}\mathbf{U}_0 \\ & + \frac{3(30 + 54c\Delta t + 28c^2\Delta t^2 + 3c^3\Delta t^3)}{5(6 + 6c\Delta t + c^2\Delta t^2)^2}\mathbf{R}_1 - \frac{3c\Delta t(9 + 9c\Delta t + c^2\Delta t^2)}{5(6 + 6c\Delta t + c^2\Delta t^2)^2}\mathbf{R}_2, \end{aligned} \quad (18)$$

with \mathbf{R}_1 and \mathbf{R}_2 are given by Eq. (19) (see below). Then for the derivation of the explicit second-order method with controllable dissipation, we will assume that $\mathbf{U}_1 = \mathbf{V}_0$ and $\mathbf{U}_2 = \mathbf{0}$ for the third term in Eq. (18). Then, from Eq. (18) we will get Eq. (20) (see below). After finding \mathbf{U}_2 from Eq. (20), vectors \mathbf{U} and \mathbf{V} at the end of the increment can be calculated (see Eqs. (12) and (15)).

The derived method reduces to the following step-by-step solution scheme.

1. For the given Δt and c (c is responsible for numerical dissipation), calculate

$$\mathbf{R}_1 = \frac{1}{\Delta t} \int_0^{\Delta t} \mathbf{R}(t)(1+ct) dt, \quad \mathbf{R}_2 = \frac{1}{\Delta t^2} \int_0^{\Delta t} 2t\mathbf{R}(t)(1+ct) dt. \quad (19)$$

2. For the given \mathbf{U}_0 and \mathbf{V}_0 , solve a system of algebraic equations

$$\begin{aligned} \mathbf{M}\mathbf{U}_2 = & -\frac{\Delta t(90 + 186c\Delta t + 129c^2\Delta t^2 + 34c^3\Delta t^3 + 3c^4\Delta t^4)}{10(6 + 6c\Delta t + c^2\Delta t^2)^2} \mathbf{K}\mathbf{V}_0 - \frac{1}{2} \mathbf{K}\mathbf{U}_0 \\ & + \frac{3(30 + 54c\Delta t + 28c^2\Delta t^2 + 3c^3\Delta t^3)}{5(6 + 6c\Delta t + c^2\Delta t^2)^2} \mathbf{R}_1 - \frac{3c\Delta t(9 + 9c\Delta t + c^2\Delta t^2)}{5(6 + 6c\Delta t + c^2\Delta t^2)^2} \mathbf{R}_2. \end{aligned} \quad (20)$$

3. Calculate the displacements and velocities \mathbf{U} and \mathbf{V} at the end of the increment

$$\mathbf{U}(\Delta t) = \mathbf{U}_0 + \mathbf{V}_0\Delta t + \mathbf{U}_2\Delta t^2, \quad \mathbf{V}(\Delta t) = \mathbf{V}_0 + 2\mathbf{U}_2\Delta t. \quad (21)$$

Eq. (17) is not used in calculations. As can be seen from the accuracy analysis (see below), scalar c does not change the order of accuracy and can vary numerical dissipation. It is interesting to mention that at $c = 0$, numerical dissipation is zero, and the method coincides with the explicit central difference method.

3.4 Accuracy analysis of the methods used at the filtering stage

Here we will present the accuracy analysis of the implicit first-order and explicit second-order TCG methods derived above. The integration of system (2)-(3) for any i from t_n to t_{n+1} by a numerical method reduces to the algebraic equations

$$\left\{ \begin{array}{c} u_i(t_{n+1}) \\ \frac{v_i(t_{n+1})}{\omega_i} \end{array} \right\} = \mathbf{A} \left\{ \begin{array}{c} u_i(t_n) \\ \frac{v_i(t_n)}{\omega_i} \end{array} \right\} + \mathbf{L}, \quad (22)$$

where \mathbf{A} is the amplification matrix, and \mathbf{L} is the load vector, $u_i(t_{n+1})$, $u_i(t_n)$ and $v_i(t_{n+1})$, $v_i(t_n)$ are the displacements and velocities at time t_{n+1} and t_n ($u_i(t_n)$ and $v_i(t_n)$ are known from the previous time increment). In the following formulas we will omit index i for u_i , v_i and ω_i for convenience. Following the standard approach, the case of free vibration (i.e., $\mathbf{L} = \mathbf{0}$ in Eq. (22)) will be considered below for the accuracy analysis.

We should mention that the spectral radius $r = \max(|r_1|, |r_2|)$ is calculated in terms of the eigenvalues r_1 and r_2 of the numerical amplification matrix \mathbf{A}_{num} and depends on the number of time increments as follows. If for one time increment the numerical amplification matrix \mathbf{A}_{num} has the eigenvalues r_1 and r_2 and the spectral

radius r , then for n uniform time steps the numerical amplification matrix is \mathbf{A}_{num}^n (it can be seen with the application of Eq. (22) from the first time step by n times at $L = 0$) with the eigenvalues r_1^n and r_2^n and the spectral radius r^n . For elastodynamics problems without physical damping, the deviation of spectral radii from unity means the introduction of numerical dissipation (the bigger the deviation, the bigger numerical dissipation). For a stable method, the spectral radius has to be smaller than unity or equal to unity with single eigenvalues.

3.4.1 The implicit first-order TCG method; see 3.2.

The application of the implicit first-order TCG method to Eqs. (2) and (3) yields the following numerical amplification matrix

$$\begin{aligned} \mathbf{A}_{num}(\Omega, m) &= \begin{bmatrix} \frac{(3+m)^2 - (2+m)\Omega^2}{(3+m)^2 + (2+m)\Omega^2} & \frac{(3+m)^2\Omega}{(3+m)^2 + (2+m)\Omega^2} \\ -\frac{(3+m)^2\Omega}{(3+m)^2 + (2+m)\Omega^2} & \frac{(3+m)^2 - (2+m)\Omega^2}{(3+m)^2 + (2+m)\Omega^2} \end{bmatrix} \\ &= \sqrt{\frac{(3+m)^2 + \Omega^2}{(3+m)^2 + (2+m)^2\Omega^2}} \begin{bmatrix} \text{Cos}(\bar{b}(\Omega, m)) & \text{Sin}(\bar{b}(\Omega, m)) \\ -\text{Sin}(\bar{b}(\Omega, m)) & \text{Cos}(\bar{b}(\Omega, m)) \end{bmatrix}, \end{aligned} \tag{23}$$

where angle \bar{b} can be expressed as $\bar{b}(\Omega, m) = \tan^{-1}(\frac{(3+m)^2\Omega^2}{(3+m)^2 - (2+m)^2\Omega^2})$ and $\Omega = \omega\Delta t$ (for simplicity, the natural frequency ω_i from Eq. (2) is used without index i). As we mentioned earlier, no physical damping matrix is used for the filtering stage, therefore the case of zero damping matrix $\mathbf{C} = \mathbf{0}$ is considered. Expanding the elements of the exact \mathbf{A} (matrix \mathbf{A} can be easily obtained by the use of the analytical solution of Eq. (2) at $\xi = 0$) and numerical \mathbf{A}_{num} (see Eq. (23)) amplification matrices into the Taylor series and comparing the corresponding terms, we can conclude that the method has the first order of accuracy. The spectral radii of the matrix \mathbf{A}_{num} for this method are shown in Figs. 1 for different m , and for one, five and ten time increments at $m = 15$. For comparison, Figs. 1 also includes the spectral radii of the amplification matrix for the implicit third-order TDG method; e.g., see Hulbert and Hughes (1990). The algorithmic damping ratios and the relative period errors are given in Fig. 2. It can be seen from Fig. 1 that the spectral radius decreases with the increase in the parameter m in functions λ_1 and λ_2 . The maximum numerical dissipation is at $m = \infty$. In this case $a_1 = \Delta t$, and \mathbf{R}_1 should be calculated analytically. If the analytical calculation of \mathbf{R}_1 at $m = \infty$ is impossible, then value $m \geq 15$ can be used because the difference in numerical dissipation for $m = \infty$ and $m \geq 15$ is not essential. The spectral radius also decreases with the increase in the number of time increments (compare curves 1, 2 and 3 for one, five and ten time steps in Fig. 1b). Let us show how the filtering stage with the implicit first-order

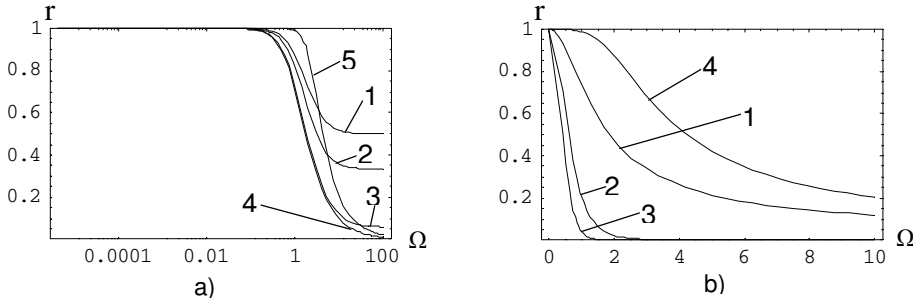


Figure 1: Spectral radii r for the implicit first-order TCG method and for the implicit third-order TDG method. Curves 1, 2, 3, and 4 in (a) correspond to the TCG method with one time increment and $m = 0, 1, 15, \infty$, respectively. Curves 1, 2, and 3 in (b) correspond to the TCG method ($m = 15$) with 1, 5 and 10 time increments. Curves 5 (a) and 4 (b) correspond to the TDG method with one time increment.

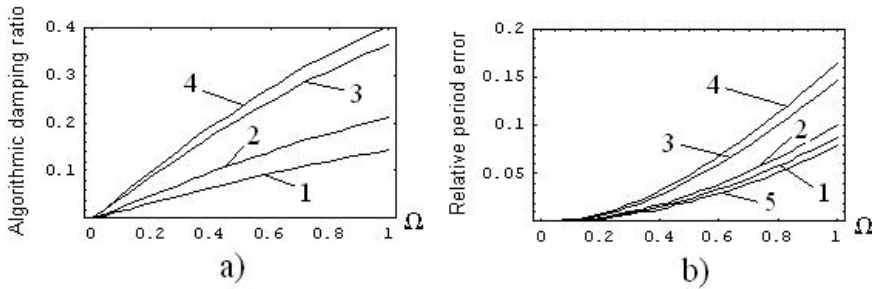


Figure 2: Algorithmic damping ratios (a) and relative period errors (b) for the implicit first-order TCG method with large numerical dissipation. Curves 1, 2, 3, 4, and 5 correspond to $m = 0, 1, 15, \infty$ and the trapezoidal rule, respectively.

TCG method modifies displacements and velocities at the even number $2n_1$ of uniform time increments (n_1 positive plus n_1 negative time increments). Using Eq. (22) with $L = 0$ and Eq. (23), we will get

$$\begin{aligned}
 \begin{Bmatrix} u(t_{2n_1}) \\ \frac{v(t_{2n_1})}{\omega} \end{Bmatrix} &= A_{num}^{n_1}(-\Omega, m) A_{num}^{n_1}(\Omega, m) \begin{Bmatrix} u(t_0) \\ \frac{v(t_0)}{\omega} \end{Bmatrix} \\
 &= \left(\frac{(3+m)^2 + \Omega^2}{(3+m)^2 + (2+m)^2 \Omega^2} \right)^{n_1} \begin{bmatrix} 1 & 0 \\ 0 & 1 \end{bmatrix} \begin{Bmatrix} u(t_0) \\ \frac{v(t_0)}{\omega} \end{Bmatrix} \\
 &= \left(\frac{(3+m)^2 + \Omega^2}{(3+m)^2 + (2+m)^2 \Omega^2} \right)^{n_1} \begin{Bmatrix} u(t_0) \\ \frac{v(t_0)}{\omega} \end{Bmatrix}. \tag{24}
 \end{aligned}$$

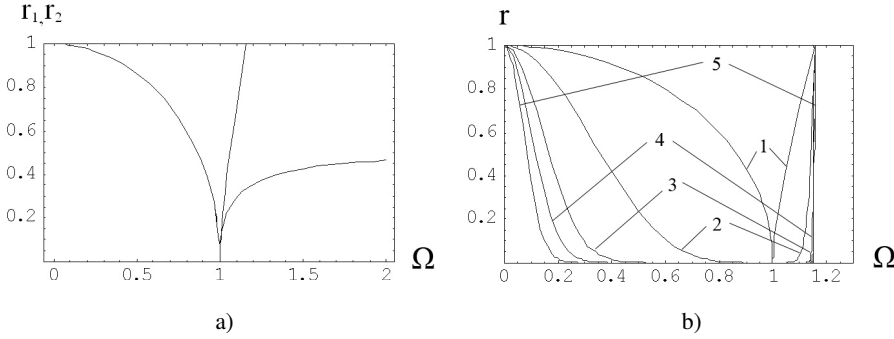


Figure 3: Eigenvalues r_1, r_2 (a) and spectral radii r (b) of the numerical amplification matrix for the explicit second-order TCG method at $d = -5.15$. Curves 1, 2, 3, 4, 5 in (b) correspond to 1, 10, 50, 100, and 200 time increments, respectively.

This means that during the filtering stage, the amplitudes of displacements and velocities for each frequency decrease by a factor $\left(\frac{(3+m)^2+\Omega^2}{(3+m)^2+(2+m)^2\Omega^2}\right)^{n_1}$ (for low frequencies ω (small Ω) this factor is close to unity, for high frequencies ω (large Ω) this factor is close to zero). For example, at $m \rightarrow \infty$ this factor is $\left(\frac{1}{1+\Omega^2}\right)^{n_1}$. Numerical examples show that the implicit first-order accurate TCG method allows the suppression of spurious high-frequency oscillations for $2n_1 = 6 \sim 10$ time steps while retaining good accuracy of the solution at low modes.

3.4.2 The explicit second-order TCG method; see 3.3.

The application of the explicit second-order TCG method to Eqs. (2) and (3) yields the following numerical amplification matrix

$$\mathbf{A}_{num}(\Omega) = \begin{bmatrix} 1 - \frac{\Omega^2}{2} & \Omega - \frac{(15+16d+3d^2)\Omega^3}{10(6+6d+d^2)} \\ -\Omega & 1 - \frac{(15+16d+3d^2)\Omega^2}{5(6+6d+d^2)} \end{bmatrix}, \quad (25)$$

where $d = c\Delta t$. Expanding the elements of the exact \mathbf{A} and numerical \mathbf{A}_{num} (see Eq. (25)) amplification matrices into the Taylor series and comparing the corresponding terms, we can conclude that the method has the second order of accuracy. The eigenvalues r_1 and r_2 of the matrix \mathbf{A}_{num} (Eq. (25)), the algorithmic damping ratios and the relative period errors for $d = -5.15$ are given in Figs. 3a and 4 for one time step. The spectral radius decreases with the increase in the number of time increments; see Fig. 3b. As can be seen from Fig. 3, at $d = -5.15$ the stability limit corresponds to $\Omega^{cr} \approx 1.2$ (e.g., for the central difference method $\Omega^{cr} = 2$, see Hughes (1987); Bathe (1996)).

Remark 1. There is an essential difference in the application of implicit and explicit methods for filtering spurious high-frequency oscillations. For the suppression of

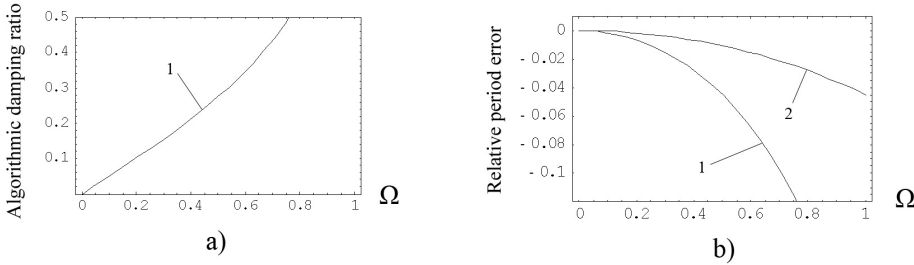


Figure 4: Algorithmic damping ratios (a) and relative period errors (b) for the explicit second-order TCG method with $d = 0$ (corresponds to the central difference method) and $d = -5.15$. Curves 1 and 2 correspond to $d = -5.15$ and $d = 0$.

spurious high frequencies starting from the frequency $\omega \geq \bar{\omega}$, the corresponding spectral radius should be small for these frequencies $r^n(\omega\Delta t) \leq \bar{r} \ll 1$ for $\bar{\omega} \leq \omega \leq \omega_{max}$ (\bar{r} is a prescribed small number, n is the number of uniform time increments, and ω_{max} is the maximum frequency of a semi-discrete system of equations). Then, assuming that r is a decreasing function of $\Omega = \omega\Delta t$ for an implicit method, the size of time increment for an implicit method has to meet the condition $r^n(\bar{\omega}\Delta t) \leq \bar{r}$ (or $\Delta t \geq \frac{r^{-1}(\bar{r}^{1/n})}{\bar{\omega}}$). For an explicit method, r is an increasing function in the vicinity of the stability limit Δt^c , therefore for explicit methods a time increment has to meet the following conditions: $r^n(\omega\Delta t) \leq \bar{r}$ for $\bar{\omega} \leq \omega \leq \omega_{max}$ and $\Delta t \leq \Delta t^c$. In many cases explicit methods may satisfy these conditions at a relatively large number n of time increments because the stability limit Δt^c is independent of the number of time steps, and for $r(\Omega) < 1$ the spectral radius $r^n(\Omega)$ significantly decreases with the increase in the number n of time increments.

4 Selection of the size of time increments for elastodynamics problems on uniform meshes

Selection of the size of time increments is an issue and is user-defined for existing time-integration methods with numerical dissipation. In this section we will suggest new formulas for selection of the size of time increments for selected time-integration methods used for the filtering stage and for basic computations. The case of zero physical damping $\mathbf{C} = \mathbf{0}$ is considered (as explained in Section 2.4, zero physical damping $\mathbf{C} = \mathbf{0}$ can be used for the filtering stage even in the case of non-zero damping $\mathbf{C} \neq \mathbf{0}$ in basic computations).

4.1 Quantification of spurious oscillations and selection of the size of time increments for the filtering stage (pre-/post-processing)

First we will consider the quantification of spurious oscillations and the selection of time increments (the amount of numerical dissipation) for the filtering stage (pre-/post-processing) for a 1-D impact problem (this problem is solved in detail in Section 5.1). The applicability of these results for other elastodynamics problems is based on the assumption that for different elastodynamics problems, the range of spurious high-frequency oscillations depends only on the size of finite elements Δx and the observation time T and is independent of initial and boundary conditions.

For the 1-D impact problem, a bar of the length L with zero initial displacements and velocities and the following boundary conditions is considered: the displacement $u(0, t) = t$ (this corresponds to the velocity $v(0, t) = v_0 = 1$) and $u(L, t) = 0$ (this corresponds to $v(L, t) = 0$); see Section 5.1 below. The exact (before the space discretization) solution for the velocities to this problem for any observation time T (until the wave front reaches to the right end) is $v(x, T) = 1$ for $0 \leq x \leq cT$ and $v(x, T) = 0$ for $cT \leq x \leq L$ (at the interface $x = cT$, a jump in the velocity occurs) where $c = \sqrt{\frac{E}{\rho}}$ is the wave velocity, E is Young's modulus and ρ is the density.

For the dimensionless coordinate $\bar{x} = \frac{x}{\Delta x}$ and the dimensionless time $\bar{t} = \frac{ct}{\Delta x}$, it is easy to show that on a uniform mesh with the element size Δx at the dimensionless observation time $\bar{T} = \frac{cT}{\Delta x}$, the exact solution of the semidiscrete (Eq. (1)) problem for the velocity $v^{semi}(\bar{x}, \bar{T})$ depends on time \bar{T} , the total number of finite elements M (or the length of the bar $L = M\Delta x$), and is independent of the size of elements and material properties. However, numerical experiments also show (e.g., see Jiang and Rogers (1990)) that the velocity $v^{semi}(\bar{x}, \bar{T})$ is practically independent of M (the exact solution $v(\bar{x}, \bar{T})$ is independent of L until the wave front reaches the right end of the bar). The explicit quantification of spurious oscillations is based on the difference $v(\bar{x}, \bar{T}) - v^{semi}(\bar{x}, \bar{T})$ between the exact solutions of the original (before the space discretization) and semidiscrete (after the space discretization) systems of elastodynamics equations (see Remark 2 below). The dimensionless observation time \bar{T} equals the number of elements $N_1 = \bar{T} = \frac{cT}{\Delta x}$ passed by the wave front. Because velocity $v^{semi}(\bar{x}, \bar{T})$ depends only on N_1 , the range of spurious high-frequency oscillations and the numerical dissipation needed for the suppression of spurious oscillations for the 1-D impact problem depend on the same parameter N_1 . At a given number of uniform time increments N , the amount of numerical dissipation of a time-integration method is determined by a time increment. Therefore, a dimensionless time increment $\Delta \bar{t} = \frac{\Delta t c}{\Delta x}$ for a time-integration method with numerical dissipation should be also a function of N_1 at given N ; i.e.,

$$\Delta \bar{t} = \bar{\alpha}(N_1, N), \quad (26)$$

where $\bar{\alpha}(N_1, N)$ is the function to be determined. Numerical experiments show that the dependence of $\bar{\alpha}(N_1, N)$ on N can be accurately approximated by the following expression $\bar{\alpha}(N_1, N) = \alpha(N_1)\Omega_{0.1}(N)$ where $\Omega_{0.1}(N)$ is the value of $\Omega = \omega\Delta t$ at which the spectral radius has the value 0.1 for the selected number N of time increments ($\Omega_{0.1}(N)$ can be found analytically from the spectral radius diagrams at different numbers N of time increments; e.g., see and Figs. 1 and 3); $\alpha(N_1)$ is the coefficient depending on the time-integration method, the order of finite elements used, and the number N_1 . Then Eq. (26) can be rewritten as follows:

$$\Delta t = \alpha(N_1) \frac{\Delta x \Omega_{0.1}(N)}{c}. \quad (27)$$

For example, for the implicit first-order TCG method with large numerical dissipation corresponding to $m = 15$ (see Sections 3.2 and 3.4.1), the following explicit expression is suggested in Idesman, Samajder, Aulisa, and Seshaiyer (2009) for the coefficient $\alpha(N_1)$:

$$\alpha(N_1) = a_1 (N_1)^{a_2} = a_1 \left(\frac{cT}{\Delta x} \right)^{a_2}, \quad (28)$$

where $a_1 = 0.279$ and $a_2 = 0.3305$ for linear elements, and $a_1 = 0.1785$ and $a_2 = 0.2357$ for quadratic elements.

Remark 1. It should be mentioned that at any specific N , the empirical coefficient $\bar{\alpha}(N_1, N)$ can be determined from numerical experiments. However, we reduce the number of numerical experiments using the analytical scaling of the spectral radii at different N . For the scaling, a point with the value of the spectral radius $r = 0.1$ on the transient part of the spectral radius diagrams is used.

Remark 2. The amount of numerical dissipation used in calculations is determined by the size of a time increment. Eqs. (27) and (28) describe the minimum necessary amount of numerical dissipation for obtaining non-oscillatory results. For the calibration of this amount (the determination of $\alpha(N_1)$), numerical experiments with the 1-D impact problem, for which all frequencies of a discrete finite element model are excited, are used in Idesman, Samajder, Aulisa, and Seshaiyer (2009). The calibration procedure is based on the minimization of the amplitudes of spurious oscillations at varying numerical dissipation (a varying time increment). The amplitudes of spurious oscillations for the velocity at observation time \bar{T} are determined as the maximum difference $e^{spur} = \max[v(\bar{x}, \bar{T}) - v^{semi}(\bar{x}, \bar{T})]$ between the exact solutions of the original and semidiscrete problems in two intervals $0 \leq \bar{x} \leq \bar{x}_1$ and $\bar{x}_2 \leq \bar{x} \leq \bar{L}$, where \bar{x}_1 and \bar{x}_2 are the coordinates of the intersection of the wave front of the solution of the semidiscrete problem with the horizontal lines $v = 0$ and $v = 1$ corresponding to the exact solution of the original problem (e.g., in Fig. 5a,

the numerical solution is close the exact solution of the semidiscrete problem). Due to the big difference between the high frequencies of the original and semidiscrete problems, the high frequencies of the semidiscrete problem mostly affect e^{spur} and are spurious. At the filtering stage, a time-integration method with numerical dissipation decreases the amplitudes of spurious oscillations. Eq. (28) indirectly quantifies the range of spurious oscillations and corresponds to the amplitudes of spurious oscillations for the velocity that do not exceed 0.25 % of the maximum value of the velocity (see Idesman, Samajder, Aulisa, and Seshaiyer (2009) for details).

Remark 3. For the 1-D impact problem, all frequencies of a semi-discrete model are excited and Eqs. (27) and (28) indirectly determines the range of spurious frequencies for all 1-D uniform meshes. For other elastodynamics problems, for which not all of the frequencies of a semi-discrete model are excited, the minimum amount of numerical dissipation described by Eqs. (27) and (28) filters the same range of high frequencies as that for the 1-D impact problem. Our experience shows that non-oscillatory numerical results are obtained with Eqs. (27) and (28) for different elastodynamics problems; i.e., the assumption that the range of spurious oscillation depends on Δx and T , is valid.

For time increments at the filtering stage of 2-D and 3-D problems on uniform quadrilateral meshes, the following modification of Eq. (27) can be used

$$\begin{aligned} \Delta t &= \max_{i,j} \left[\alpha \left(\frac{c_i T}{\Delta x_j} \right) \right] \max_{i,j} \left[\frac{\Delta x_j}{c_i} \right] \Omega_{0.1}(N) \\ &= a_1 \left[\frac{\max_i (c_i) T}{\min_j (\Delta x_j)} \right]^{a_2} \frac{\max_j (\Delta x_j)}{\min_i (c_i)} \Omega_{0.1}(N), \end{aligned} \quad (29)$$

where $\max_i (c_i) = \max(c_1, c_2)$ and $\min_i (c_i) = \min(c_1, c_2)$ ($i = 1, 2$) are the maximum and minimum values between the velocities of the longitudinal wave $c_1 = \sqrt{\frac{E(1-\nu)}{\rho(1+\nu)(1-2\nu)}}$ and the transversal wave $c_2 = \sqrt{\frac{E}{2\rho(1+\nu)}}$, Δx_j are the dimensions of finite elements along the axes x_j ($i = 1, 2$ for the 2-D problems and $i = 1, 2, 3$ for the 3-D problems). Eq. (29) is based on Eq. (27) with the selection of the maximum size of a time increment with respect to the longitudinal and transversal waves, and the dimensions of a finite element along the coordinate axes. For uniform meshes with linear and quadratic quadrilateral elements in the 2-D and 3-D cases, the coefficients a_1 and a_2 obtained for the 1-D case (see Eq. (28)) are used.

Remark. We used the following motivation for the formulation of Eq. (29) for the 2-D and 3-D cases. We assumed that harmonic plane waves of different frequencies propagating along the coordinate axes of a uniform finite element mesh can detect all spurious frequencies in numerical solutions that should be damped out. Each

displacement component of the harmonic plane wave in the 3-D case meets the 1-D wave equation with the wave velocity c_1 or c_2 (e.g., see Nowacki (1975)); i.e., in the 2-D and 3-D cases we check Eq. (27) for each component of the harmonic plane wave in all directions x_j for the wave velocities c_1 and c_2 . Eq. (29) is the necessary condition for the selection of time increments in the 2-D and 3-D cases.

4.2 Selection of the size of time increments for basic computations

For the stage of basic computations, the semidiscrete equations should be integrated accurately for long-term time integration, and time-integration methods with zero numerical dissipation can be used (see Section 2). Here, for the selection of the size of time increments in the case of zero physical damping $\xi = 0$ (or $\mathbf{C} = \mathbf{0}$), we will use the exact, closed-form a-priori error estimator derived in our paper Idesman (2010). This estimator describes the exact error in time during long-term time integration by the trapezoidal rule (the most accurate second-order method), and by the implicit fourth-order and the sixth-order accurate TCG methods with zero numerical dissipation proposed in Idesman (2007a). We should mention that in the case of zero numerical dissipation, the high-order TCG methods coincide with the known high-order accurate methods presented in Fung, Fan, and Sheng (1998); Kanapady and Tamma (2003); Gross, Betsch, and Steinmann (2005) and correspond to the diagonal of the Padé approximation table.

Remark. In the case of non-zero damping $\xi \neq 0$ (or $\mathbf{C} \neq \mathbf{0}$), the accuracy of numerical results at the stage of basic computations can be estimated by the comparison of numerical results calculated for the same observation time at different numbers of time increments. However, such an approach is very time consuming. Therefore, at small damping and in the absence of other error estimators, the global error estimator described below for zero damping can be used as an approximation of the global error needed for the selection of time increments in the case of small damping.

In our paper Idesman (2010), for time integration of each frequency ω we derived the exact expression for the global relative error e in displacements and velocities, and the following simplified formulas for this error at small uniform time increments Δt and the observation time T :

$$e \approx \frac{1}{12} T \omega^3 \Delta t^2 \quad \text{for the trapezoidal rule,} \quad (30)$$

$$e \approx \frac{1}{720} T \omega^5 \Delta t^4 \quad \text{for the fourth-order accurate TCG method,} \quad (31)$$

$$e \approx \frac{1}{100800} T \omega^7 \Delta t^6 \quad \text{for the sixth-order accurate TCG method.} \quad (32)$$

Because the spurious high-frequency oscillations are filtered at the pre- or post-processing stage, it is not necessary for the spurious high frequencies to be integrated accurately at the stage of basic computations. The cut-off frequency ω_c will be selected as $\omega_c = \frac{\Omega_{0.1}(N)}{\Delta t}$ where frequencies $\omega > \omega_c$ are filtered at the pre- or post-processing stage; i.e., the cut-off frequency ω_c corresponds to the spectral radius $r = 0.1$ for a time integration method used at the filtering stage. For 1-D elastodynamics problems at the given observation time T and the size of finite elements Δx , the cut-off frequency ω_c can be selected as follows (see Eqs. (27) and (28)):

$$\omega_c(\Delta x, T) = \frac{\Omega_{0.1}(N)}{\Delta t} = \frac{c}{a_1 \Delta x} \left(\frac{cT}{\Delta x} \right)^{-a_2}. \quad (33)$$

Then, at basic computations we select the size of a time increment for which the frequency ω_c is integrated with the prescribed accuracy $e = \varepsilon_{tol}$ according to Eqs. (30) - (32); i.e., a time increment for basic computations can be selected as

$$\Delta t(\Delta x, T) \approx \frac{\sqrt{12\varepsilon_{tol}}}{\omega_c \sqrt{T} \omega_c} \quad \text{for the trapezoidal rule,} \quad (34)$$

$$\Delta t(\Delta x, T) \approx \frac{\sqrt[4]{720\varepsilon_{tol}}}{\omega_c \sqrt[4]{T} \omega_c} \quad \text{for the fourth-order accurate TCG method,} \quad (35)$$

$$\Delta t(\Delta x, T) \approx \frac{\sqrt[6]{100800\varepsilon_{tol}}}{\omega_c \sqrt[6]{T} \omega_c} \quad \text{for the sixth-order accurate TCG method.} \quad (36)$$

Because the trapezoidal rule and the considered high-order TCG methods with zero numerical dissipation are more accurate than other implicit and explicit time-integration methods of the same order of accuracy, then time increments for other second- and high-order time-integration methods should be equal to or smaller than those given by Eqs. (34) - (36). According to Eqs. (30) - (32), at the same time increments Δt and the observation times T , frequencies $\omega < \omega_c$ are integrated with higher accuracy ($e < \varepsilon_{tol}$). The error given by Eqs. (30) - (32) for each mode can differ from the total error of a numerical solution which is a linear combination of different modes. Therefore, it is recommended that the tolerance ε_{tol} for the mode with frequency ω_c be select from the analysis of the total error of a numerical solution (this can be done by numerical experiments). E.g., numerical experiments for the 1-D impact problem show that the use of time increments calculated by Eqs. (33) - (36) with $\varepsilon_{tol} = 0.05$ for linear elements and $\varepsilon_{tol} = 0.15$ for quadratic elements yields final numerical results close to that (within the tolerance 0.25%

for the amplitudes of spurious oscillations after the filtering stage; see Section 4.1) obtained with very small time increments at the stage of basic computations. We should also mention that the selection of the cut-off frequency as $\omega_c = \frac{\Omega_{0.1}(N)}{\Delta t}$ does not affect the generality of numerical results because according to Eqs. (34) - (36) the cut-off frequency ω_c can be combined with the prescribed accuracy ε_{tol} , which is found from numerical experiments.

For 2-D and 3-D elastodynamics problems, the size of time increments for the stage of basic computations can be calculated from Eqs. (34) - (36) using $\omega_c = \frac{\Omega_{0.1}(N)}{\Delta t}$ with Δt calculated for the filtering stage according to Eq. (29).

Remark 1. The size of time increments at the stage of basic computations given by Eqs. (33) - (36) for the selected time-integration methods can be used for all elastodynamics problems. However, for structural dynamics for which only low frequencies are excited, a time increment given by Eqs. (34) - (36) may be very conservative (very small) and will lead to an unnecessary increase in computation time. Therefore, for structural dynamics, a lower cut-off frequency ω_c can be used in Eqs. (34) - (36) (its value should be known from the problem formulation).

Remark 2. We can also use another scenario for the selection of time increments for long-term integration. Assume that at time integration by the trapezoidal rule or by the high-order TCG methods with some selected uniform time increments Δt_s , we have obtained accurate numerical results at the short observation time T_s . Then, in order to keep the same error e at large observation times T_l , according to Eqs. (30) - (32), time increments can be calculated as follows: $\Delta t_l = \Delta t_s \sqrt{T_s/T_l}$, $\Delta t_l = \Delta t_s \sqrt[4]{T_s/T_l}$ and $\Delta t_l = \Delta t_s \sqrt[6]{T_s/T_l}$ for the second-order, the fourth-order and the sixth-order accurate TCG methods, respectively; i.e., the time increment Δt_l for the large observation time should be decreased by the corresponding factor for each time-integration method.

5 Numerical examples

The new technique and the TCG methods for the filtering stage are implemented into the finite element code FEAP (Zienkiewicz and Taylor (2000)). Numerical solutions to 1-D and 2-D axisymmetric elastodynamics problems will be considered in the paper. The implicit TCG method with large numerical dissipation applied for pre- or post-processing will be used with $m = 15$; see Sections 3 and 3.4.

5.1 Impact of an elastic bar against a rigid wall

This 1-D example is related to the impact of an elastic bar of the length $L = 4$ against a rigid wall. It is known that the application of the traditional semidiscrete

methods to this problem leads to oscillations in velocities and stresses due to the spurious high-frequency response; e. g. see Hulbert and Hughes (1990). The numerical solutions to this problem with a propagating discontinuity in velocity and stress will demonstrate the effectiveness of the two-stage time-integration procedure and the implicit and explicit TCG methods used for filtering spurious oscillations. We will show that the new approach yields accurate non-oscillatory results for

- linear and quadratic finite elements on uniform meshes (Fig. 5), emphasizing that at the same number of degrees of freedom, quadratic elements are more accurate than linear elements (Figs. 5d and 6a);
- non-uniform finite element meshes with linear and quadratic elements (Fig. 6a);
- the two-stage time-integration procedure with pre- and post-processing.

We will also show that the recommendations for the selection of a time increment for explicit methods suggested in textbooks on finite elements are incorrect.

Young's modulus is chosen to be $E = 1$ and the density to be $\rho = 1$. The following boundary conditions are applied: the displacement $u(0, t) = t$ (this corresponds to the velocity $v(0, t) = v_0 = 1$) and $u(4, t) = 0$ (this corresponds to $v(4, t) = 0$). Initial displacements and velocities are zero; i.e., $u(x, 0) = v(x, 0) = 0$. At any observation time, the analytical solution for the velocity (stress) to this problem is a piecewise constant function with a jump at the wave front (the wave front travels with the constant velocity $c = \sqrt{E/\rho}$).

Fig. 5 shows the numerical results obtained by the two-stage time-integration procedure, which includes basic computations with the implicit fourth-order accurate TCG method and post-processing with the implicit first-order accurate TCG method (10 time increments, $\Omega_{0,1} = 0.81$, see Fig. 1b). Two uniform meshes with 50 quadratic and 100 linear finite elements (i.e., meshes with the same numbers of degrees of freedom) were used for these calculations. The sufficiently small size of time increments ($\Delta t = 0.005$) for basic calculations was applied. Therefore, for the selected observation times, the error in time for basic computations was very small and can be neglected for both meshes.

Remark. Any implicit or explicit first- and higher-order time-integration method can be used in basic computations with very small increments because at very small time increments the numerical results are close to the exact solution of the semi-discrete system, Eq. (1), and are independent of a time-integration method.

From Fig. 5a it follows that for basic computations the slope of the wave front decreases with the increase in the observation time (or more precisely, with the increase in the number of elements N_1 passed through by the wave front). Similar numerical results were reported in Jiang and Rogers (1990). The velocity distri-

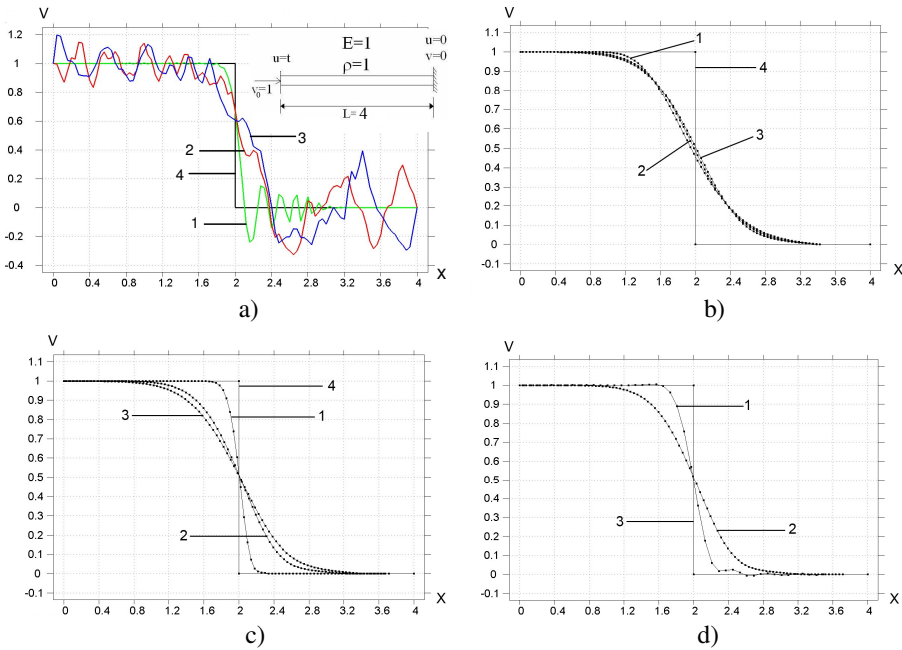


Figure 5: Velocity distribution along the bar for long-term behavior calculated on uniform meshes with 100 linear 2-node finite elements (a,b,c, and curve 2 in d) and with 50 quadratic 3-node finite elements (curve 1 in d). (a), (b) and (c and d) correspond to the solutions obtained by the fourth-order accurate TCG method with zero numerical dissipation, by the two-stage time-integration procedure with post-processing based on uniform time increments of the same sizes (with fixed $\alpha = 4.34$) at different observation times, and by the two-stage time-integration procedure with post-processing based on uniform time increments of different sizes (with varying α) at different observation times, respectively; see the text for explanations. Curves 1, 2 and 3 in (a, b, c) correspond to the observation times $T = 2, 98$ and 162 , respectively. Curves 1 and 2 in (d) correspond to the observation times $T = 98$. Curves 3 in (d) and 4 in (a, b, c) correspond to the analytical solutions at the observation times $T = 2, 98$ and 162 .

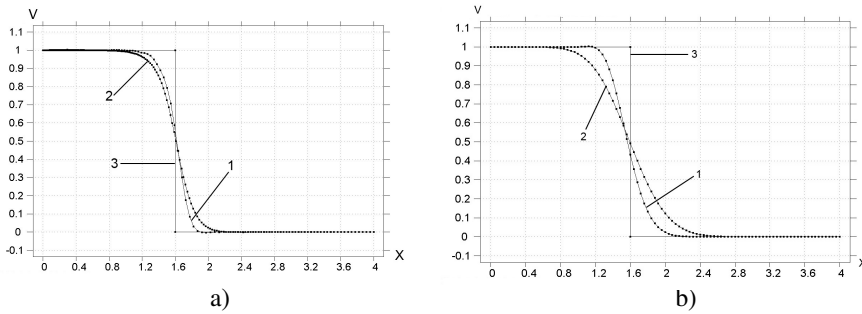


Figure 6: Velocity distribution along the bar at time $T = 22.4$ (long-term behavior) calculated on non-uniform meshes (a) with 100 quadratic 3-node (1) and with 200 linear 2-node (2) finite elements and on a uniform mesh with 100 linear 2-node finite elements (b). The two-stage time-integration procedure with post-processing by the implicit first-order TCG method was used in (a) and for curve 1 in (b). The first-order TCG method with numerical dissipation ($m = 0$) was used for all calculations for curve 2 in (b); see the text for explanations. Curve 3 corresponds to the analytical solution at time $T = 22.4$.

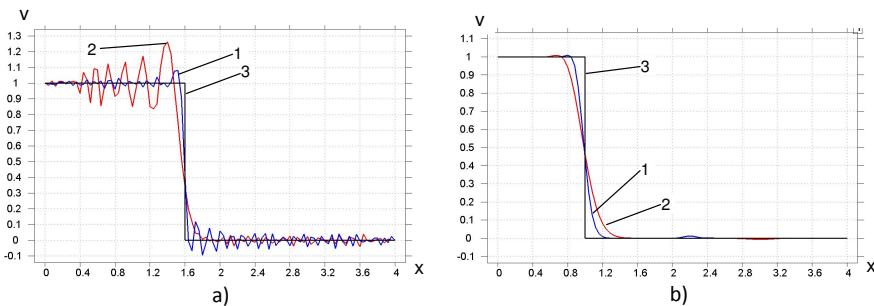


Figure 7: Velocity distribution along the bar for long-term behavior calculated on a uniform mesh with 100 quadratic 3-node finite elements. The two-stage time-integration procedure with the explicit central-difference method for basic computations until time $T = 22.4$ and post-processing with the explicit second-order TCG method until time $T = 23$ was used. Curves 1 and 2 correspond to the solutions obtained with different uniform time increments for basic computations; $\Delta t_1 = 0.0064$ for curve 1 and $\Delta t_2 = 2.5\Delta t_1 = 0.016$ for curve 2. Curve 3 corresponds to the analytical solutions at the observation time $T = 22.4$ (a) and $T = 23$ (b).

butions in Fig. 5a have a great number of spurious oscillations. Therefore, it is difficult to compare the accuracy of numerical results obtained on different meshes and at different observation times (the selected observation times correspond to many reflections of the elastic wave from the ends of the bar). However, the spurious oscillations can be damped out by post-processing. Using the large value of the coefficient $\alpha = 4.34$ for linear elements (it corresponds to $T = 162$ according to Eq. (28)), the smooth non-oscillatory solutions are obtained in Fig. 5b for all selected times. These numerical solutions correspond to the position of the wave front in the middle of the bar and are close to each other. However, for smaller observation times, accuracy of the solutions with linear elements can significantly be improved by the selection of smaller numerical dissipation (smaller values of α); see Fig. 5c (according to Eq. (28), $\alpha = 1.02, 3.68, 4.34$ was used for curves 1, 2 and 3, respectively). For quadratic elements, similar results were obtained. Fig. 5d shows the comparison of the numerical results obtained at the same observation time and with the uniform meshes consisting of linear and quadratic elements. As we can see from Fig. 5d, at the same numbers of degrees of freedom, quadratic elements yield much more accurate results. Similar results were also obtained on non-uniform meshes; see Fig. 6a. Non-uniform meshes with the same ratio $\Delta x_{max}/\Delta x_{min} = 7.2$ were used for the calculations shown in Fig. 6a with linear and quadratic elements.

Remark. For the implicit first-order TCG method with large numerical dissipation, a non-oscillatory solution can be obtained even with one time increment ($N = 1$). However, numerical experiments show that the slope of the wave front at $N = 1$ is much more diffusive than that at $N = 6 \sim 10$. The selection of the optimal number of N is considered in Idesman, Samajder, Aulisa, and Seshaiyer (2009).

Fig. 6b shows the comparison of the two-stage time-integration procedure with existing approaches based on the application of a time-integration method with numerical dissipation for all calculations. The application of the implicit first-order TCG method with numerical dissipation ($m = 0$) for all calculations yields the non-oscillatory solution for the considered impact problem; see Fig. 6b, curve 2. However, the two-stage time-integration procedure yields much more accurate results; see curve 1 in Fig. 6b and the introduction for the explanations.

The instantaneous application of the finite velocity $v_0 = 1$ at the left end of the bar excites a high-frequency response of the bar at the initial time only. Therefore, according to the two-stage time-integration procedure, pre-processing or post-processing can be applied to this problem for filtering spurious oscillations. Numerical results show that the two-stage time-integration procedure with pre-processing yields non-oscillatory solutions close to those in Figs. 5(c, d) and 6 obtained with post-processing; i.e., for the 1-D impact problem, the sequence of the application of basic computations and the filtering stage does not affect numerical results (see

also Idesman, Samajder, Aulisa, and Seshaiyer (2009) for additional examples).

Next, we will show the application of the two-stage time-integration procedure with explicit time-integration methods. The following numerical result also emphasizes the importance of accurate long-term integration of elastodynamics problems in basic computations. The 1-D impact problem was solved by the application of the two-stage time-integration procedure with the explicit central difference method for basic computations and the explicit second-order TCG method with large numerical dissipation ($d = -5.15$) for post-processing; see also Sections 3.3 and 3.4.2. A uniform mesh with 100 quadratic finite elements was used. A lumped mass matrix and two different uniform time increments were selected for basic computations $\Delta t_1 = 0.0064$ and $\Delta t_2 = 2.5\Delta t_1 = 0.016$ (the value $\Delta t_2 = 0.016$ is close to the stability limit). Velocity distributions along the bar at time $T = 22.4$ are shown in Fig. 7a for the central difference method. As expected, oscillatory numerical solutions were obtained; see curves 1 and 2 in Fig. 7a. However, due to error accumulation during long-term integration, the wave front in curve 2 is more diffusive than that in curve 1 in Fig. 7a. For post-processing with the explicit TCG method ($d = -5.5$), the time increment should be selected close to the stability limit and was taken to be $\Delta t = 0.009$. In this case, 67 and 223 time increments were used for post-processing in order to obtain non-oscillatory numerical solutions 1 and 2 in Fig. 7b.

As we can see, due to more accurate long-term integration with time increments $\Delta t_1 = 0.0064$ (much smaller than the stability limit) during basic computations, the more accurate non-oscillatory solution was obtained after post-processing (compare curves 1 and 2 in Fig. 7b). These results also have fundamental significance for explicit time-integration methods. They show the incorrectness of recommendations for the selection of time increments for explicit methods described in many textbooks on the finite element method; see the discussion in Section 6.

It is necessary to mention that basic computations with the explicit central difference method can be combined with post-processing based on the implicit first-order TCG method with numerical dissipation; see the numerical solutions of 3-D elastodynamics problems in our paper Idesman, Schmidt, and Foley (2010). We repeated calculations for the 1-D impact problem (similar to those described in Fig. 7), using basic computations performed by the central difference method with small time increments $\Delta t_1 = 0.0064$ until time $T = 23$, and using post-processing performed by the implicit first-order TCG method with 10 time increments $\Delta t = 0.0277$ calculated according to Eqs. (27) and (28). The distribution of the velocity after post-processing at time $T = 23$ practically coincides with curve 1 in Fig. 7b.

Remark. The number, N , of time increments necessary for post-processing with the explicit TCG method, can be approximated with the help of Eq. (27) as follows. Time increments of the explicit TCG method used for the filtering stage are close

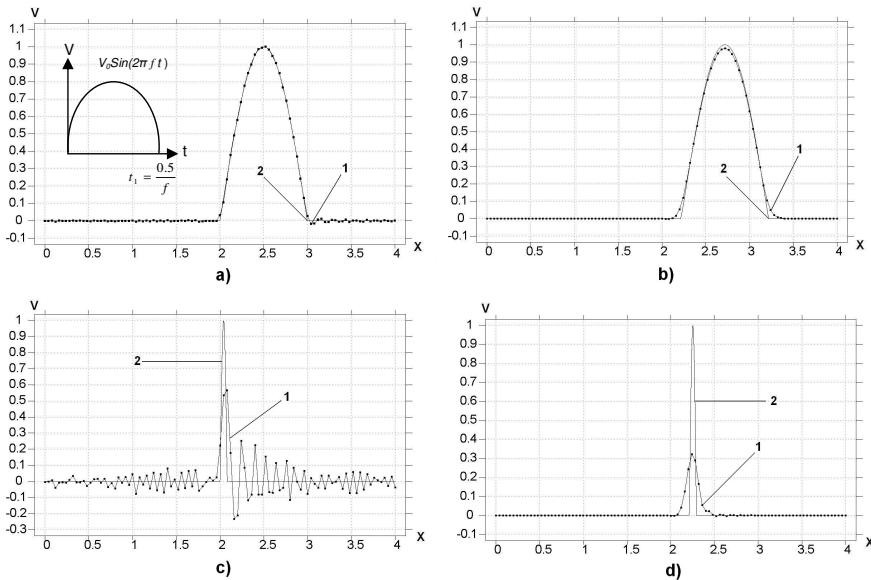


Figure 8: Velocity distribution along the bar for the low-frequency ($f = 1$ (a, b)) and high-frequency ($f = 12.5$ (c, d)) pulses calculated on a uniform mesh with 100 quadratic 3-node finite elements after basic computations (a, c) and after post-processing (b, d). Curves 1 and 2 correspond to the numerical and analytical solutions, respectively. The following times are considered: $T = 11$ (a), $T = 11.2172$ (b), $T = 10.08$ (c), $T = 10.2928$ (d).

to the stability limit. Then from Eq. (27) it follows that for the explicit TCG method $\Omega_{0,1}(N) = \frac{c\Delta t}{\alpha(N_1)\Delta x}$ where $\alpha(N_1)$ is calculated according to Eq. (28) for the implicit first-order TCG method. With the inverse function $N(\Omega_{0,1})$ calculated from the spectral radii diagrams for the explicit TCG method, the number of time increments N can be found. A detailed study of the calculation of the number, N , at the filtering stage for the explicit TCG method as well as an approximation of $N(\Omega_{0,1})$ as a function of $\Omega_{0,1}$ will be considered elsewhere.

5.2 Propagation of sinusoidal velocity pulses of low and high frequencies through an elastic bar

This problem is used in order to demonstrate the application of Eqs. (27) and (28), which prescribe the minimum necessary amount of numerical dissipation, to the simplest 1-D elastodynamics problems. The same bar and the same properties as those in Section 5.1 are considered. The following boundary conditions are

applied: at the left end the displacement $u(0,t) = v_0[1 - \text{Cos}(2\pi ft)/(2\pi f)]$ (this corresponds to the sinusoidal velocity pulse $v(0,t) = v_0 \text{Sin}(2\pi ft)$) for $t \leq t_1$, and $F(0,t) = 0$ for $t \geq t_1$; at the right end $F(4,t) = 0$, where f is the frequency of the pulse, v_0 is the amplitude of the pulse ($v_0 = 1$ in calculations), the duration of the pulse t_1 is selected as $t_1 = 0.5/f$, F is the external force. Initial displacements and velocities are zero; i.e., $u(x,0) = v(x,0) = 0$. According to the analytical solution, the sinusoidal pulse (with the shape of a half-wave sine) propagates from the left end to the right end and back, without a change in shape and amplitude, and with a constant velocity $c = 1$. It is easy to show that the finite element solution to this problem in the dimensionless coordinates depends on the number of finite elements per wave length and the length of the bar L , and is independent of the dimensionless frequency of the applied pulse. However, if the same finite element mesh is used for pulses of different frequencies, then a sinusoidal pulse of high frequency includes a smaller number of finite elements per wave length than a sinusoidal pulse of low frequency. A uniform finite element mesh with 100 quadratic 3-node elements is used for pulses of two different frequencies $f = 1$ and $f = 12.5$. For basic computations, the trapezoidal rule with a small time $\Delta t = 0.0001$ is used for both frequencies (for the selected observation times indicated in Fig. 8, the numerical results for basic computations do not vary with the further decrease in a time increment Δt). For the low frequency ($f = 1$), 25 finite elements per pulse length along the x -axis is used; and for the high frequency ($f = 12.5$), 2 finite elements per pulse length along the x -axis is used. Fig. 8 shows the solutions for high and low frequency pulses after basic computations (a, c) and after post-processing by the implicit first-order TCG method with 10 time increments with $\Delta t = 0.02172$ (b) and $\Delta t = 0.02128$ (d). These time increments are calculated according to Eqs. (27) and (28) for the selected observation times that correspond to two reflections of the pulses from the left and right ends. As we could expect, for the low-frequency pulse, a numerical solution after basic computations is close to the analytical solution with small, spurious high-frequency oscillations before and after the pulse; see Fig. 8a. After post-processing, a non-oscillatory numerical solution is obtained (however, a small deviation from the analytical solution can be seen due to post-processing with numerical dissipation); see Fig. 8b. For the high-frequency pulse, the numerical solution includes numerous spurious oscillations after basic computations and differs essentially from the analytical solution; see Fig. 8c. After post-processing, a non-oscillatory numerical solution is obtained; see Fig. 8d. Despite the fact that the solution after post-processing differs from the analytical solution, it does not have spurious oscillations. For a more accurate numerical solution for a high-frequency pulse, a mesh refinement should be used.

These 1-D problems (see also Section 5.1) show that for non-oscillatory results,

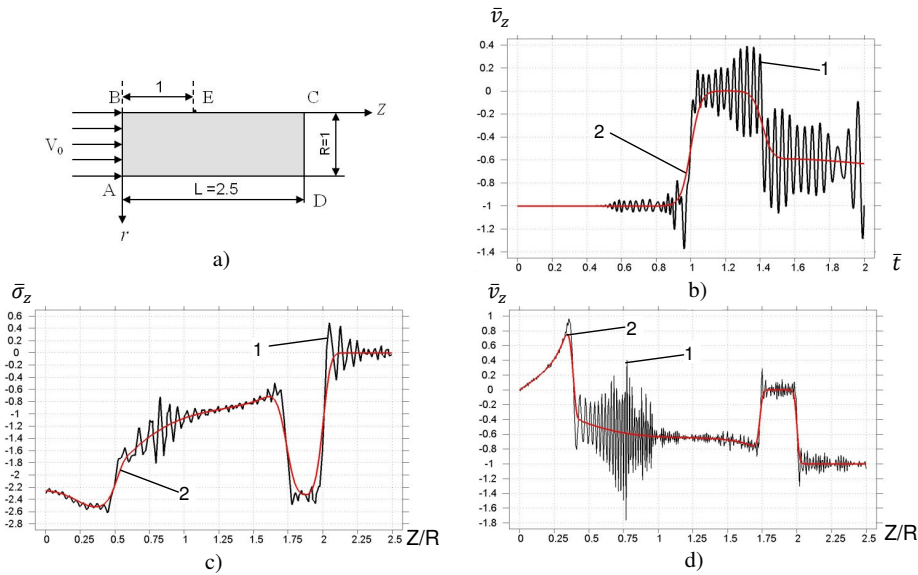


Figure 9: Impact of an elastic cylinder against a rigid wall (a). The evolution of the axial velocity \bar{v}_z (b) at point E ($\bar{r} = 0$, $\bar{z} = 1$; see (a)) and the distribution of the axial stress $\bar{\sigma}_z$ (c) and velocity \bar{v}_z (d) along the dimensionless axial coordinate $\bar{z} = z/R$ and the fixed dimensionless radial coordinate \bar{r} ($\bar{r} = 0.05$ for (c) and $\bar{r} = 0$ for (d)) at dimensionless time $\bar{T} = c_1 t/R = 2$. Curves 1 correspond to basic computations without the filtering stage. Curves 2 correspond to pre-processing plus basic computations (b) and basic computations plus post-processing (c, d). Uniform meshes with 5000 (b, c) and 80000 (d) quadratic Q_9 elements were used.

the amount of numerical dissipation can be selected independently of the boundary and initial conditions and is determined by the dimensions of finite elements and the observation time; see Eqs. (27) and (28).

5.3 Impact of an elastic cylinder against a rigid wall

This axisymmetric problem will be used for the demonstration of the effectiveness of the new approach in the multi-dimensional case with the presence of longitudinal and transversal elastic waves. A cylinder of length $L = 2.5$ and radius $R = 1$ is considered. The z -axis is the axis of revolution. Young's modulus is chosen to be $E = 1$, Poisson's ratio $\nu = 0.3$, and the density to be $\rho = 1$. The following boundary conditions are applied: along boundary AB $u_n = t$ (this corresponds to velocity $v_n = v_0 = 1$) and $\tau_n = 0$; along boundaries CD and AD $\sigma_n = 0$ and $\tau_n = 0$; along boundary BC $u_n = 0$ and $\tau_n = 0$, where u_n , v_n , and σ_n are the normal displacements,

velocities and the tractive forces, respectively; τ_n are the tangential tractive forces. Initial displacements and velocities are zero; i.e., $u(r, z, 0) = v(r, z, 0) = 0$. To compare a numerical solution of the problem with the approximation of the analytical solution derived in Vales, Moravka, Brepta, and Cerv (1996), the dimensionless coordinates ($\bar{r} = \frac{r}{R}$ and $\bar{z} = \frac{z}{R}$), the dimensionless time $\bar{t} = \frac{t c_1}{R}$ and the normalized displacements $\bar{u}_i = \frac{u_i c_1}{R v_0}$, velocities $\bar{v}_i = \frac{v_i}{v_0} - 1$, stresses $\bar{\sigma}_{ij} = \frac{\sigma_{ij} c_1 (1+\nu)(1-2\nu)}{\nu E v_0}$ and strains $\bar{\epsilon}_{ij} = \frac{\epsilon_{ij} c_1}{v_0}$ ($i, j = r, z$) are used, where $c_1 = \sqrt{\frac{E(1-\nu)}{\rho(1+\nu)(1-2\nu)}}$ is the longitudinal wave rate. The dimensionless observation time is chosen to be $\bar{T} = 2$. The problem was solved on three uniform meshes with $50 \times 100 = 5000$, $100 \times 200 = 20000$ and $200 \times 400 = 80000$ quadratic 9-node elements. A consistent mass matrix was used in all calculations. The trapezoidal rule with uniform time increments $\Delta \bar{t} = 0.0002$ was applied for basic computations. At these small time increments, the error in time was small and could be neglected. The application of the explicit fourth-order TCG method (see Idesman, Schmidt, and Sierakowski (2008)) with uniform time increments $\Delta \bar{t} = 0.0002$ yielded practically the same results for basic computations. Without the filtering stage, the numerical results include many spurious high-frequency oscillations in stresses and velocities on the coarse and fine meshes; see curves 1 in Fig. 9. These oscillations spoil the numerical solution and make it impractical. Because for this problem, the boundary conditions excite a high-frequency response of the cylinder at the initial time only (similar to the previous 1-D problem), pre- or post-processing can be used for the filtering of the spurious oscillations. Here, for the filtering stage, we use the implicit first-order TCG method with 10 uniform time increments calculated according to Eq. (29) ($\Delta t = 0.0141, 0.00832, 0.0049$ for meshes with 5000, 20000 and 80000 finite elements, respectively). Non-oscillatory smooth results were obtained with pre- or post-processing; see curves 2 in Fig. 9. It is necessary to mention that the filtering stage with the explicit TCG method ($d = -5.5$) requires 500 time increments ($\Delta t = 0.00048$) on the fine mesh with 80000 elements and yields the non-oscillatory numerical results close to curves 2 in Fig. 9 (pre- or post-processing with the same sizes of time increments yield practically the same results).

Remark. We should mention that for elastodynamics problems, the convergence of numerical solutions in the energy norm may lead to very inaccurate results at local points due to spurious oscillations. For example, the solutions in Fig. 9 obtained by the TCG method without numerical dissipation (curves 1) are more accurate in the energy norm than the non-oscillatory solutions (curves 2 in Fig. 9) obtained by the two-stage time-integration procedure, because in the former case the energy is exactly conserved, and in the latter case there is small energy dissipation due to numerical dissipation at the filtering stage.

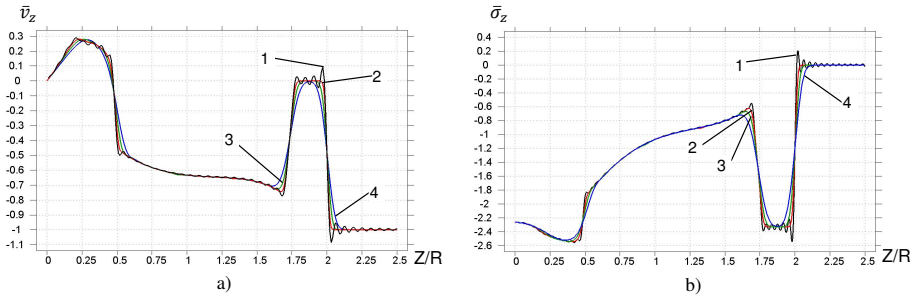


Figure 10: The distribution of the dimensionless velocity \bar{v}_z (a) and axial stress $\bar{\sigma}_z$ (b) along the dimensionless axial coordinate $\bar{z} = z/R$ and the fixed dimensionless radial coordinate \bar{r} ($\bar{r} = 0.05$) at dimensionless time $\bar{T} = c_1 t/R = 2$. Curve 1 is the approximation of the analytical solution. Curves 2, 3 and 4 correspond to the numerical solutions obtained with the two-stage time-integration procedure on uniform meshes with 80000, 20000, and 5000 quadratic $Q9$ elements, respectively.

Fig. 10 shows the convergence of non-oscillatory numerical results, obtained with the two-stage time-integration procedure (basic computations plus post-processing) at mesh refinement, to the approximation of the analytical solution derived in Vales, Moravka, Brepta, and Cerv (1996) using the Laplace transform. The approximate analytical solution (curves 1 in Fig. 10) has spurious oscillations due to Gibbs phenomena. The oscillations can clearly be seen for the range $2 < z/R < 2.5$ in Fig. 10 where the exact stresses and velocities are zero (a non-disturbed domain). The numerical solutions (curves 2-4) do not have these oscillations.

6 Concluding remarks

The new two-stage time-integration procedure for elastodynamics suggested in the paper allows fast, accurate and non-oscillatory solutions for elastodynamics problems. In contrast to existing approaches, the new technique does not require any guesswork for the selection of numerical dissipation or artificial viscosity and retains the accuracy of the basic solution at low modes. The new expression related to the selection of necessary numerical dissipation (see Eqs. (27)-(29)) allows accurate non-oscillatory results with no need for interaction between a computer code and users. Because the approach is applied to the semi-discrete formulation of elastodynamics, it can be combined with any method used for space discretization such as the finite element method, the finite difference method, the spectral element method, the boundary element method, the smoothed particle hydrodynamics method and many others.

The application of the new approach to several test elastodynamics problems also shows that quadratic finite elements yield more accurate results than linear finite elements at the same numbers of degrees of freedom. It is known that high-order spatial discretization in space is effective for wave propagation problems (e.g., see Komatitsch, Barnes, and Tromp (2000)). However, in contrast to existing approaches that yield spurious oscillations, the new approach allows convergence of non-oscillatory numerical results with high-order discretization in space.

The two-stage time-integration procedure also suggests a new look at requirements for the selection of time-integration methods for elastodynamics. Because the two-stage time-integration procedure consists of two different stages, different criteria should be used for the selection of a time-integration method for each of these stages. For basic computations, a method that accurately integrates semi-discrete equations is needed, and spurious oscillations are allowed; i.e., numerical dissipation is not required at this stage. For example, it is known that the trapezoidal rule is the most accurate method among all second-order accurate methods for elastodynamics. This method does not have numerical dissipation and at zero physical damping $\mathbf{C} = \mathbf{0}$ conserves the total energy, and the linear and angular momentum of a mechanical system during time integration. According to the new approach, the trapezoidal rule is the only method for the time integration of linear elastodynamics at the stage of basic computations if an implicit second-order method will be used. If an explicit method will be used, then at the same computational costs, a method with the smallest asymptotic error (according to accuracy analysis) should be used for basic computations. Due to the error accumulation, high-order accurate methods (with zero or very small numerical dissipation) are more effective for long-term integration than second-order accurate methods.

Existing approaches to the selection of a time-integration method for elastodynamics include some contradictory criteria such as obtaining high-order accurate results and the introduction of numerical dissipation needed for the suppression of spurious oscillations (numerical dissipation usually degrades the accuracy of numerical solutions); e.g., see Hughes (1987). In Zhou, Tamma, and Sha (2005) the selection of a time-integration method by design based on the combination of some contradictory criteria is suggested for implicit second-order accurate methods (because just one method is used for all calculations). This means that a selected time-integration method depends on the problems considered and the objectives of calculations. The new approach is free of these contradictions, yields the most accurate numerical results for elastodynamics problems, and may have the slightly larger computational cost compared to existing approaches (due to the additional filtering stage). The new approach can be equally applied to wave propagation and structural dynamics problems (for structural dynamics, the filtering stage may be omitted if high modes

of semidiscrete equations are not excited).

For the filtering stage, a method with large numerical dissipation (artificial viscosity) is necessary for filtering spurious high-frequency oscillations. Because a small number of time increments for implicit methods is used at this stage, even a method of the first-order of accuracy is competitive. We have developed new implicit and explicit TCG methods with large numerical dissipation that effectively damp out spurious oscillations. However, it is possible that a more effective method with numerical dissipation (that requires a smaller number of time increments) or another computationally cheaper filter can be developed for the filtering stage.

In contrast to the recommendations in textbooks on finite elements, for long-term integration, the size of time increments for explicit methods should be much smaller than the stability limit (rather than close to it) and should depend on the total number of time increments; see Fig. 7. Only in the case of the 1-D linear wave equation and a uniform mesh consisting of 2-node linear finite elements, does the explicit central difference method with a time increment equal to the stability limit yield the exact solution of the wave equations (the error in time is compensated by the error in space; e.g., see Hughes (1987)). In other cases (2-D or 3-D problems, high-order finite elements) the size of a time increment should depend on the total number of time increments for an accurate solution.

One scenario of the two-stage time-integration procedure (basic computations plus post-processing) can be directly implemented with known non-linear elastodynamics formulations for elastoplastic and non-linear elastic materials (see Simo, Tarnow, and Wong (1992); Simo and Tarnow (1992); Gonzalez (2000); Betsch and Steinmann (2001); Gross, Betsch, and Steinmann (2005); Armero (2006)) where a time-integration method with zero numerical dissipation is used in order to preserve the conservation of energy, and linear and angular momentum. However, spurious high-frequency oscillations appear with these non-linear formulations for wave propagation problems. This follows from the fact that for linear materials (as a particular case of non-linear materials), the approaches described in these papers are reduced to the trapezoidal rule and will yield spurious high-frequency oscillations similar to those in Figs. 5a, 8c and 9. Then, the spurious oscillations appearing in the above-mentioned non-linear formulations can be suppressed using the post-processing stage of the suggested two-stage time-integration procedure. To generalize, basic computations plus post-processing can be applied to non-linear problems if at mesh refinement the exact solution of a semi-discrete dynamics problem described by a system of non-linear ordinary differential equations in time, converges in some norms to the solution of the original dynamics problem described by non-linear partial differential equations. In this case, very accurate time integration can be used in basic computations, and the filtering of spurious os-

cillations which appear due to space discretization can be done at post-processing. However, for non-linear problems the quantification of the range of spurious high frequencies and the amount of numerical dissipation needed for their filtering is an issue and requires additional study. Nevertheless, spurious frequencies in numerical solutions for elastic components of non-linear structures can be removed by the post-processing of these components separately from the entire non-linear structure using a time integration method with the amount of numerical dissipation given by Eqs. (27) - (29). It follows from the fact that linear and non-linear components of a structure interact through the boundary conditions at the common boundaries but the range of spurious oscillations in the elastic components is independent of the boundary conditions (see section 4.1).

Acknowledgement: The research has been supported in part by the Air Force Research Lab, Eglin (contract # FA8651-08-D-0108). The technical assistance of Himadri Samajder (Texas Tech University) is very much appreciated.

References

- Abedi, R.; Petracovici, B.; Haber, R. B.** (2006): A space-time discontinuous galerkin method for linearized elastodynamics with element-wise momentum balance. *Computer Methods in Applied Mechanics and Engineering*, vol. 195, pp. 3247–3273.
- Armero, F.** (2006): Volume-preserving energy-momentum schemes for isochoric multiplicative plasticity. *Computer Methods in Applied Mechanics and Engineering*, vol. 195, no. 37-40, pp. 4862–4889.
- Bathe, K. J.** (1996): *Finite element procedures*. Prentice-Hall Inc., Upper Saddle River, New Jersey.
- Betsch, P.; Steinmann, P.** (2001): Conservation properties of a time fe method—part ii: Time-stepping schemes for non-linear elastodynamics. *Int. Journal for Numerical Methods in Engineering*, vol. 50, no. 8, pp. 1931–1955.
- Bonelli, A.; Bursi, O. S.** (2001): Explicit predictor-multicorrector time discontinuous galerkin methods for linear dynamics. *Journal of Sound and Vibration*, vol. 246, no. 4, pp. 625–652.
- Chien, C. C.; Wu, T. Y.** (2000): Improved predictor/multi-corrector algorithm for a time-discontinuous galerkin finite element method in structural dynamics. *Computational Mechanics*, vol. 25, no. 5, pp. 430–437.

- Fung, T. C.; Fan, S. C.; Sheng, G.** (1998): Mixed time finite elements for vibration response analysis. *Journal of Sound and Vibration*, vol. 213, no. 3, pp. 409–428.
- Gonzalez, O.** (2000): Exact energy and momentum conserving algorithms for general models in nonlinear elasticity. *Computer Methods in Applied Mechanics and Engineering*, vol. 190, no. 13-14, pp. 1763–1783.
- Govoni, L.; Mancuso, M.; Ubertini, F.** (2006): Hierarchical higher-order dissipative methods for transient analysis. *International Journal for Numerical Methods in Engineering*, vol. 67, no. 12, pp. 1730–1767.
- Gross, M.; Betsch, P.; Steinmann, P.** (2005): Conservation properties of a time fe method. part iv: Higher order energy and momentum conserving schemes. *International Journal for Numerical Methods in Engineering*, vol. 63, no. 13, pp. 1849–1897.
- Grosu, E.; Harari, I.** (2007): Stability of semidiscrete formulations for elastodynamics at small time steps. *Finite Elements in Analysis and Design*, vol. 43, no. 5, pp. 533–542.
- Holmes, N.; Belytschko, T.** (1976): Postprocessing of finite element transient response calculations by digital filters. *Computers and Structures*, vol. 6, no. 3, pp. 211–216.
- Hughes, T. J. R.** (1987): *The Finite Element Method: Linear Static and Dynamic Finite Element Analysis*. Prentice- Hall, Englewood Cliffs, NJ,.
- Hulbert, G. M.** (1992): Discontinuity-capturing operators for elastodynamics. *Computer Methods in Applied Mechanics and Engineering*, vol. 96, no. 3, pp. 409–426.
- Hulbert, G. M.; Hughes, T. J. R.** (1990): Space-time finite element methods for second-order hyperbolic equations. *Computer Methods in Applied Mechanics and Engineering*, vol. 84, no. 3, pp. 327–348.
- Idesman, A. V.** (2007): A new high-order accurate continuous galerkin method for linear elastodynamics problems. *Computational Mechanics*, vol. 40, pp. 261–279.
- Idesman, A. V.** (2007): Solution of linear elastodynamics problems with space-time finite elements on structured and unstructured meshes. *Computer Methods in Applied Mechanics and Engineering*, vol. 196, pp. 1787–1815.
- Idesman, A. V.** (2010): A new exact, closed-form a-priori global error estimator for second- and higher-order time integration methods for linear elastodynamics. *International Journal for Numerical Methods in Engineering*, pp. 1–22 (submitted).

Idesman, A. V.; Samajder, H.; Aulisa, E.; Seshaiyer, P. (2009): Benchmark problems for wave propagation in elastic materials. *Computational Mechanics*, vol. 43, no. 6, pp. 797–814.

Idesman, A. V.; Schmidt, M.; Foley, J. R. (2010): Finite element simulation of 3-d wave propagation and impact elastodynamics problems. *Wave motion*, pp. 1–25 (submitted).

Idesman, A. V.; Schmidt, M.; Sierakowski, R. L. (2008): A new explicit predictor-multicorrector high-order accurate method for linear elastodynamics. *Journal of Sound and Vibration*, vol. 310, pp. 217–229.

Jiang, L.; Rogers, R. J. (1990): Effects of spatial discretization on dispersion and spurious oscillations in elastic wave propagation. *International Journal for Numerical Methods in Engineering*, vol. 29, no. 6, pp. 1205–1218.

Kanapady, R.; Tamma, K. K. (2003): On a novel design of a new unified variational framework of discontinuous/continuous time operators of high order and equivalence. *Finite Elements in Analysis and Design*, vol. 39, no. 8, pp. 727–749.

Komatitsch, D.; Barnes, C.; Tromp, J. (2000): Simulation of anisotropic wave propagation based upon a spectral element method. *Geophysics*, vol. 65, no. 4, pp. 1251–1260.

Krenk, S. (2001): Dispersion-corrected explicit integration of the wave equation. *Computer Methods in Applied Mechanics and Engineering*, vol. 191, pp. 975–987.

Krenk, S. (2006): State-space time integration with energy control and fourth-order accuracy for linear dynamic systems. *International Journal for Numerical Methods in Engineering*, vol. 65, no. 5, pp. 595–619.

Kunthong, P.; Thompson, L. L. (2005): An efficient solver for the high-order accurate time-discontinuous galerkin (tdg) method for second-order hyperbolic systems. *Finite Elements in Analysis and Design*, vol. 41, no. 7-8, pp. 729–762.

Li, X. D.; Wiberg, N. E. (1998): Implementation and adaptivity of a space-time finite element method for structural dynamics. *Computer Methods in Applied Mechanics and Engineering*, vol. 156, pp. 211–229.

Mancuso, M.; Ubertini, F. (2003): An efficient integration procedure for linear dynamics based on a time discontinuous galerkin formulation. *Computational Mechanics*, vol. 32, no. 3, pp. 154–168.

Nowacki, W. (1975): *Dynamic Problems of Thermoelasticity*. Springer.

Palaniappan, J.; Haber, R. B.; Jerrard, R. L. (2004): A spacetime discontinuous galerkin method for scalar conservation laws. *Computer Methods in Applied Mechanics and Engineering*, vol. 193, pp. 3607–3631.

Simo, J.; Tarnow, N. (1992): The discrete energy-momentum method. conserving algorithms for nonlinear elastodynamics. *ZAMP*, vol. 43, pp. 757–793.

Simo, J.; Tarnow, N.; Wong, K. (1992): Exact energy-momentum conserving algorithms and symplectic schemes for nonlinear dynamics. *Computer Methods in Applied Mechanics and Engineering*, vol. 100, no. 1, pp. 63–116.

Vales, F.; Moravka, S.; Brepta, R.; Cerv, J. (1996): Wave propagation in a thick cylindrical bar due to longitudinal impact. *JSME International Journal, Series A*, vol. 39, no. 1, pp. 60–70.

Valliappan, S.; Wang, Y. C. (1991): Advances in computational mechanics applied to wave propagation problems. In Siriwardane; Zaman(Eds): *Computer Methods and Advances in Geomechanics, volume 1*, pp. 347–362.

Wang, Y. C.; Murti, V.; Valliappan, S. (1992): Accuracy of the newmark method in transient analysis of wave propagation problems. *Earthquake Engineering and Structural Dynamics*, vol. 21, pp. 987–1004.

Xing, Y.; Shu, C. (2006): High order well-balanced finite volume weno schemes and discontinuous galerkin methods for a class of hyperbolic systems with source terms. *Journal of Computational Physics*, vol. 214, pp. 567–598.

Zhou, X.; Tamma, K. K.; Sha, D. (2005): Design spaces, measures and metrics for evaluating quality of time operators and consequences leading to improved algorithms by design - illustration to structural dynamics. *International Journal for Numerical Methods in Engineering*, vol. 64, no. 14, pp. 1841–1870.

Zienkiewicz, O. C.; Taylor, R. L. (2000): *The Finite Element Method*. Butterworth-Heinemann, Oxford, UK.